JOURNAL OF GEOPHYSICAL RESEARCH, VOL. 114, C07003, doi:10.1029/2008JC005016, 2009

Dynamics of wind-driven upwelling and relaxation between Monterey Bay and Point Arena: Local-, regional-, and gyre-scale controls

James M. Pringle[1] and Edward P. Dever[2]

Received 14 August 2008; revised 10 February 2009; accepted 7 April 2009; published 2 July 2009.

[1] In north and central California, equatorward winds drive equatorward flows and the upwelling of cold dense water over the shelf during the midspring and summer upwelling season. When the winds temporarily weaken, the upwelling flows between Point Reyes and Point Arena "relax," becoming strongly poleward over the shelf. Analytical and numerical models are used to describe the effect of alongshore variability of winds, bathymetry, and basin-scale pressure gradients on the strength of upwelling and its relaxation. Alongshore winds weaken to the south of Point Reyes, and the shelf becomes narrower from Point Reyes to Monterey Bay. Both of these lead to reduced upwelling at and to the north of Point Reyes, causing an alongshore gradient of temperature and density on the shelf. These alongshore gradients lead to an along-isobath pressure gradient over the shelf that drive the relaxation flows. A simple analytical model is used to explain the dynamics, magnitude, and structure of the relaxation flows. The modeling also suggests that the depth of origin of the upwelled waters, and thus their temperature, is controlled by the along-isobath pressure gradient that exists over the continental slope. This along-slope pressure gradient is also responsible for the California undercurrent in this region. This pressure gradient is not generated in a model of the Californian coast extending from 32°N to 42°N and integrated for several months, suggesting it is caused by dynamics whose spatial or temporal scales are larger than the Californian coast and/or longer than several months.

Citation: Pringle, J. M., and E. P. Dever (2009), Dynamics of wind-driven upwelling and relaxation between Monterey Bay and Point Arena: Local-, regional-, and gyre-scale controls, *J. Geophys. Res.*, *114*, C07003, doi:10.1029/2008JC005016.

1. Introduction

[2] Northern California from Point Reyes to Point Arena is an archetypal upwelling center. It was first described in detail during the 1981–1983 Coastal Ocean Dynamics Experiment (CODE) [*Winant et al.*, 1987] augmented by super CODE [*Strub et al.*, 1987]. The region was revisited during the 1988–1989 Shelf Mixed Layer Experiment (SMILE) [*Dever and Lentz*, 1994] and as part of the 1987–1989 Northern California Coastal Circulation Study (NCCCS) [*Largier et al.*, 1993]. More recently, the 2000–2003 Wind Events and Shelf Transport (WEST) study was undertaken to examine how the circulation dynamics of this upwelling center control the biology [*Largier et al.*, 2006]. All of these studies included moored arrays to examine the oceanic response to meteorological forcing on scales from tens of km (CODE, SMILE, WEST) to several hundred km (super CODE, NCCCS).

[3] As in most other upwelling regions, there is a high correlation between local and regional winds and the alongshore flow [e.g., *Winant et al.*, 1987]. The strongest correlations occur between local alongshore flows and the winds about 200 km to the south, at lags consistent with coastal-trapped wave (CTW) theory [*Denbo and Allen*, 1987; *Chapman*, 1987]. Regional limited-domain numerical models capture this correlation but tend to overpredict the equatorward alongshore flow from upwelling favorable winds and under-predict the poleward flows that occur during wind relaxation events. For example, the modeled standard deviations of the alongshore currents are larger than observed by *Gan and Allen* [2002a] at midshelf and deeper at the central CODE site, while *Cervantes and Allen* [2006] have larger than observed variability near the coast near Point Reyes. In both models, the poleward flow that develops when the alongshore winds relax is either missing or smaller than the observations, and is limited to a region too close to the shore near and to the north of Point Reyes (discussed below). They also predict colder upwelled waters than observed. *Gan and Allen* [2002a] suggest that these flaws are caused by their use of spatially uniform winds and the lack of poleward pressure gradients in the ocean basins adjacent to their model domain.

[4] These model-data discrepancies suggest that alongshore variability on scales larger than these model domains control the strength of upwelling and relaxation in this upwelling system. This variation may be in the wind forcing

[1]Department of Earth Sciences, UNH, Durham, New Hampshire, USA.
[2]College of Oceanic and Atmospheric Sciences, Oregon State University, Corvallis, Oregon, USA.

0148-0227/09/2008JC005016$09.00

[e.g., *Csanady*, 1978; *McCreary and Chao*, 1985; *Chapman*, 1987], in the bathymetry [*Pringle*, 2002; *Janowitz and Pietrafesa*, 1982], or in the basin-scale circulation adjacent to the coast [*Wright*, 1986; *Hill*, 1995]. The three-dimensional variability appears as an along-shelf pressure gradient present in diagnoses of the along-shelf momentum balance [*Lentz*, 1987; *Brown et al.*, 1987; *Lentz*, 1994; *Dever*, 1997] and in 2-D models of circulation [*Zamudio and Lopez*, 1994]. This alongshore pressure gradient is similar in magnitude to the alongshore wind stress, and forces a poleward flow in the absence of an equatorward wind.

[5] Spatial variation in wind forcing has long been recognized as a cause of alongshore variability. Its importance has been explored over a large range of timescales and space scales. Perhaps the most familiar spatial and temporal scales are the meteorological synoptic scales (about 100 km and a week) that force CTW's. CTW models of remote wind forcing [*Chapman*, 1987; *Denbo and Allen*, 1987; *Chapman et al.*, 1988] confirm that on the west coast of North America, winds to the south of a point affect conditions at that point. The phase speed of the observed response to remote forcing is consistent with CTW's. These models capture the sense of the relationship between local and remote alongshore winds and the alongshore currents, and produce forecasts of the currents that are well correlated with the observations. In the Point Reyes region, they indicate that much of the wind forcing important to local circulation is located around Pigeon Point/Monterey Bay, some 250 km to the south. However, CTW theory underpredicts the magnitude of alongshore currents at midshelf and the magnitude of the temperature response [*Chapman*, 1987]. This could be due to either the linearization of the temperature evolution equation or the large number of modes needed to predict temperature and currents [*Clarke and VanGorder*, 1986; *Zamudio and Lopez*, 1994]. These errors are likely to be exacerbated by the many O(1) changes in shelf width on scales much less than the CTW wavelength, which will scatter wave energy into high, and poorly resolved, modes [*Wilkin and Chapman*, 1990]. The CTW models also fail to predict the poleward currents that exist in the absence of equatorward winds, the ''upwelling relaxation'' response [*Send et al.*, 1987].

[6] Alongshore variation in wind forcing on longer timescales (seasonal, annual or long-term mean) also forces three dimensional variability in coastal upwelling systems. *McCreary* [1981] examined the effect of spatial variation in mean winds with a linear analytical model. The model had idealized vertical mixing, a flat bottom, and simplified surface and bottom boundary conditions to enable analytical solutions. It also had a meridional coastline with alongshore wind forcing along a single stretch of that coastline. The idealized wind forcing was inspired by the winds along the California coast. Within the region of wind forcing, an equatorward surface current was generated with a poleward undercurrent. The maximum current magnitudes occurred near the northern limit of wind forcing; however, this basic current structure extended several hundred km north of the wind-forced region. *McCreary and Chao* [1985] and *McCreary et al.* [1987] later expanded the model to include a continental shelf and wind stress curl. The continental shelf weakened the poleward undercurrent because it induced a barotropic along-slope pressure gradient. Positive wind stress curl near the coast strengthened the poleward undercurrent.

[7] Spatial variability in wind forcing, including wind stress curl, has also been studied in the southern California Bight. *Oey* [1999] identified the near coast poleward flow observed in the region with an equatorward weakening of wind stress curl. *Oey et al.* [2004] and *Dong and Oey* [2005] showed the modeled response was quite sensitive to wind stress curl on scales less than 50 km and incorporation of short-scale winds improved model agreement with observed time series.

[8] In addition to wind variability, spatial variation in bathymetry contributes to three-dimensional variability in coastal upwelling systems [*Allen*, 2000; *Janowitz and Pietrafesa*, 1982]. For example, in an idealized model of wind-driven flows along a coast with alongshore varying bathymetry, *Pringle* [2002] finds that if the shelf widens in the direction of coastal-trapped wave propagation and if the shelf width change is O(1), upwelling favorable winds will setup poleward pressure gradients whose magnitude will be of the same order as the wind stress. These conditions exist between Point Reyes and Monterey Bay. However, the *Pringle* [2002] model is barotropic, and forced only by the winds. When the winds cease, the alongshore pressure gradient goes away, and no poleward relaxation flow occurs. While this model can explain how changes in shelf width can modify the strength of upwelling near Point Reyes and lead to some of the observed along-isobath pressure gradients, it cannot explain the observed upwelling relaxation.

[9] In this paper we use a variety of numerical model domains, wind forcing regimes and initial hydrographic conditions to quantify the importance of remote and local forcing in this region and the effects of alongshore variability in winds and bathymetry. We evaluate these models on the basis of measurements taken during WEST. These models suggests that alongshore density variation caused by the widening of the shelf north of Monterey Bay and alongshore variation in wind strength lead to along-isobath pressure gradients over the shelf which persist after the alongshore winds cease. These pressure gradients are the main causes of the poleward upwelling relaxation flow in the Point Reyes/CODE region. Basin-scale pressure gradients are not needed to predict shelf flows in this region. However, the modeling also suggests that the along-slope pressure gradient over the slope and farther offshore controls the depth of the origin of the upwelled water, and thus the temperature, salinity and nutrients on the shelf during upwelling. These pressure gradients are not generated by even the largest model domain used here, suggesting that they are caused by basin- or gyre-scale dynamics, or by dynamics on timescales longer than the two month model integrations described below.

[10] The upwelling processes that occur over the central and northern California shelf are also observed in other upwelling regions. Some of the results found here should carry over to these other regions, while other results will depend on conditions particular to the central and northern California shelves. In the conclusion, the broader applicability of these results will be discussed. We hope this analysis will refine our understanding of how large-scale

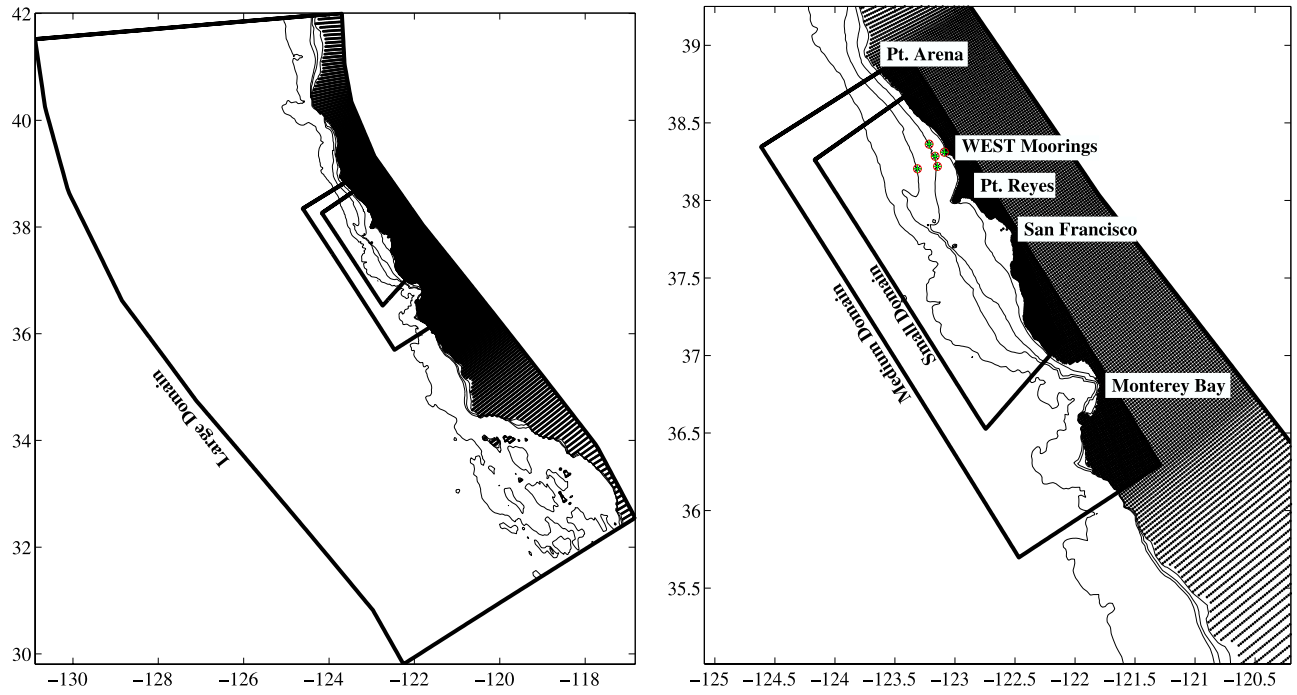

Figure 1. (left) The three model domains and the 40, 90, 130, and 1200 m isobaths within them. (right) Close-up of model domain in vicinity of CODE and WEST regions, including location of WEST moorings. The three model domains used and their names are also shown.

variations in winds and bathymetry affect coastal wind-driven circulation.

2. Ocean Model and Data

2.1. Current and Wind Data

[11] The modeling here is focused on simulating the observations made as part of the WEST project from 1 May through 30 June of 2001, and associated satellite observation of sea surface temperature and Coastal Ocean Dynamics Applications Radar-based estimates of surface currents. We use currents and meteorological data from a trio of moorings that make up the central line of the WEST experiment on the 40, 90, and 130 m isobath, shown in Figure 1. Documentation of the data from these moorings can be found in the papers by *Largier et al.* [2006] and *Dever et al.* [2006].

[12] Winds for forcing the model was taken from two regional atmospheric models, the Coupled Ocean/Atmosphere Mesoscale Prediction System (COAMPS) model of NRL Monterey [*Haack et al.*, 2005], and the Fifth-Generation National Center for Atmospheric Research/Penn State Mesoscale Model (MM5) model of *Koracin et al.* [2004]. For the 2001 period, COAMPS converted their estimates of wind speed to stress with the *Louis* [1979] scheme, while MM5 11 m winds were converted to stress with the *Large and Pond* [1981] scheme. Both of these models use a series of nested grids, and the finest available grid for each model is used. The smallest-scale data around Point Reyes for MM5 was 3 km, while for COAMPS it was 9 km. For both models the largest scale of data was 27 km, but this data was only used well away from the Point Arena to Monterey Bay region. The winds yielded largely similar results, with COAMPS providing slightly better model/data correlations. So for most of the discussion only the COAMPS runs were used. Wind taken from one point in the atmospheric models, the location of the central 90 m WEST site, will be used to test the effects of spatially uniform winds.

2.2. Details of the Numerical Model

[13] The modeling presented here has benefited greatly from the work of *Gan and Allen* [2002b], *Gan and Allen* [2002a], and *Cervantes and Allen* [2006]. Where possible, we used similar parameters to theirs in order to facilitate intercomparisons. The model is version 2.2 of the Regional Ocean Modeling System (ROMS), with minor modifications. Vertical mixing is parameterized by the Mellor-Yamada 2.5 closure with the Kantha-Clayson mixing length scheme [*Mellor and Yamada*, 1982; *Kantha and Clayson*, 1994]. Surface heat fluxes were taken from the May–June 2001 average of the fluxes from the central WEST mooring, as described by *Cervantes and Allen* [2006]. The shortwave radiation in was 275.4 W m^{-2}, and the total heat flux into the ocean was 80 W m^{-2}. Bathymetry was taken from the NGDC 3 second coastal relief data set and the STRM30_PLUS V2.0 data set where the NGDC data set did not have data. For each model the bathymetry was smoothed to remove length scales smaller than twice the local model resolution, and then subsampled to the model grid by linear interpolation. Any place where the change in depth between adjacent grid points normalized by the depth was greater than 0.2 was further smoothed [*Mellor et al.*, 1994]. Depths were truncated to 1400 m. One model run was made with a deeper maximum depth of 2800 m, and in it currents on the shelf were unchanged and temperature on the shelf was no more

than 0.05°C colder than in the model with a smaller maximum depth.

[14] A series of model runs were also made with a bathymetry that only depended on the distance from shore, in order to investigate the role of alongshore variation of the shelf width. In these runs, the coastal depth was 10 m, the shelf sloped linearly offshore to a shelf break depth of 140 m over a shelf width of 26 km, followed by a slope which reached 1400 m depth over the next 26 km offshore. Offshore of the slope the depth was a uniform 1400 m.

[15] The model was run on a series of model domains, to judge the effect of domain size (Figure 1). The smallest domain had a resolution of about 0.5 km. The middle domain had a resolution of 1.5 km, but results were checked for numerical convergence with a 0.7 km run. For the largest domain, the model grid is 10 km at the northern and southern boundaries, 2 km in the central Monterey/Point Arena region, and a linear interpolation of model resolution between these areas. Convergence was examined with runs in which the model resolution in the region near Point Reyes was twice as fine, and no significant changes were seen in the alongshore velocity or temperature fields presented below. The largest domain grid is 340 by 163 grid points.

[16] Initial stratification was typical of the WEST region, and is the same as that used by *Cervantes and Allen* [2006]. In some runs, temperature and salinity were treated as passive tracers that did not modify density, in order to understand the barotropic dynamics of the model runs. In those runs, vertical momentum mixing was set to produce 7 m thick Ekman layers, and the same mixing parameters were used for the tracers.

[17] As in the paper by *Cervantes and Allen* [2006], a third-order upwind-biased advection scheme was used for the tracer and momentum evolution equations, and a splines density Jacobian scheme was used for the pressure gradient calculation [*Shchepetkin and McWilliams*, 2003].

[18] The northern and southern boundary conditions are inspired by *Gan and Allen* [2005]. The boundary conditions are meant to capture upwelling dynamics on a Northern Hemisphere west coast, where the momentum dynamics are dominated by the northward propagation of CTW's from the southern boundary while the generally equatorward wind-driven flows will advect temperature and salinity from the northern boundary into the model domain. To capture these dynamics, two-dimensional model runs with no alongshore variability are run for the northern and southern boundaries with the wind forcing appropriate at those boundaries. This is, essentially, an assumption that the ocean is alongshore uniform in bathymetry, dynamics, and forcing outside of the model domain. On the southern boundary, the two-dimensional solution is used to set the free surface and momentum fields of the three-dimensional model. Experiments with schemes that only clamped the momentum when the phase speed was outward [e.g., *Gan and Allen*, 2005] led to occasional instabilities associated with spurious short, southward propagating disturbances, and so were not used. On the southern and northern boundaries, temperature and salinity were set to the two dimensional model solutions on inflow. For the northern boundary, radiation conditions were used on outflow, with weak nudging to the two-dimensional solution as in the paper by *Marchesiello et al.* [2003]. The major failing of these open boundary conditions is that there is excessive upwelling on the two-dimensional northern boundary model (for reasons discussed below), allowing excessively cold upwelled water to be advected into the model domain. This is especially a problem in the largest model domain where there is the largest discrepancy between the 2D and interior solutions. Therefore the integration is stopped after 30 June to avoid contaminating the solutions of interest in the central part of the model domain. Otherwise, the solution in the interior of the model is remarkably insensitive to the choice of boundary conditions on the northern boundary, consistent with the propagation direction of CTW in this domain. (The periodic boundary conditions of *Gan and Allen* [2002a] and *Cervantes and Allen* [2006] could not be used because spatially varying winds on timescales of 1 to several days will excite strong and artificial CTW resonances if periodic boundary conditions are used.)

[19] The offshore boundary was implemented with a wall and an 8 grid point wide sponge layer which relaxed all fields back to their initial values.

[20] Along with the realistic model runs, several runs are made with idealized winds. The "pulse wind" model runs are forced with the mean 1 May to 30 June 2001 winds from the COAMPS model; the winds are linearly ramped up over 1 day, are applied through day 20, and then linearly ramped down in 1 day to zero wind. The model is run for a further 20 days. Some model runs were also made in which there either was a latitudinal gradient in the initial salinity and temperature fields at depths greater than 100 m, or a uniform inflow over the shelf on the southern boundary. As will be seen below, both of these lead to a realistic California undercurrent, and a modification of the water masses that are advected onto the shelf from offshore during upwelling.

3. A Summary of Model Results

[21] Before using the model results to understand upwelling dynamics in this system, it is useful to compare the various model runs to the observations, in order to get a sense of the behavior of the ocean and the reliability of the models. Tables 1, 2, and 3 and Figures 2 and 3 compare the depth-averaged alongshore currents in the observations with the various model runs. We concentrate on the depth-averaged currents because the alongshore flows are largely coherent over depth in both the models and the observations [*Dever et al.*, 2006].

[22] The base model run is made on the largest domain and is forced by the COAMPS winds with their full spatial variability. Correlations between the alongshore depth-averaged velocity in the base model run and the observed currents range from 0.93 at 90 m depth to 0.49 at the 130 m mooring (correlations about 0.36 are significant at the 95% level). Correlations with the other model runs are nearly as good, though in general slightly less at the midshelf and inner shelf and better on the outer shelf, and these correlations are similar to those found in other models of the area [*Gan and Allen*, 2002a; *Cervantes and Allen*, 2006]. The lower correlation at the offshore 130 m mooring in the base case is caused by an eddy which impinges on this mooring on year day 170 and thereafter, driving a flow that does not

Table 1. Model and Current Meter Statistics for the Depth-Averaged Alongshore Flow at 40 m[a]

Data Source	Mean (cm s^{-1})	SD (cm s^{-1})	R
Large domain/full variability	1.9	8.2	0.72
Large domain/uniform topography	−5.7	13.2	0.90
Large domain/uniform winds	−23.7	13.6	0.73
Large domain/no baroclinicity	−2.41	7.21	0.78
Medium domain	1.73	13.9	0.59
Small domain	−17.3	13.2	0.65
Large domain/MM5 winds	−8.9	11.8	0.68
Large domain/meridional isopycnal tilt and CUC	3.57	7.2	0.74
Current meter	−1.25	7.14	

[a]The Pearson correlation coefficient R is significant at the 95% level when $R \geq 0.36$. SD, standard deviation.

Table 2. Model and Current Meter Statistics for the Depth-Averaged Alongshore Flow at 90 m[a]

Data Source	Mean (cm s^{-1})	SD (cm s^{-1})	R
Large domain/full variability	−4.4	8.3	0.93
Large domain/uniform topography	−12.3	9.5	0.86
Large domain/uniform winds	−24.0	8.8	0.74
Large domain/no baroclinicity	−8.5	7.4	0.91
Medium domain	−11.8	13.7	0.76
Small domain	−21.1	7.1	0.54
Large domain/MM5 winds	−9.1	11.1	0.75
Large domain/meridional isopycnal tilt and CUC	−2.3	7.2	0.88
Current meter	−1.2	7.7	

[a]The Pearson correlation coefficient R is significant at the 95% level when $R \geq 0.36$.

agree with the current meter moorings. If the correlation is calculated from 1 May to 20 June, the correlation is 0.79. This is not to excuse the model; eddies from offshore often affect this depth [*Largier et al.*, 1993; *Lentz*, 1987], and to the extent these eddies are nondeterministic, they will degrade the ability of the model to simulate the circulation. Other estimates of wind-driven motions also tend to have decreased correlation with observations at this location [e.g., *Chapman*, 1987; *Dever et al.*, 2006]. In *Kaplan et al.*'s [2005] comparison of HF radar-derived surface currents and winds, there is a sharp drop-off of the correlation between winds and currents at and offshore of the 130 m mooring. It may well be that over the outer shelf and slope, only assimilative models can improve correlations over wind-forced models because of the stochastic nature of the eddies.

[23] Correlation is not the only important measure of a model's skill; it is also important to compare the mean and standard deviation of the currents in the models to observations. In general, the base model with its large domain and realistic winds does a reasonable job in predicting the mean and standard deviation of the alongshore flows. However, the models with smaller domains, or the models forced with uniform winds, tend to overpredict the mean equatorward flow and, on the midshelf and inner shelf, overpredict the variance of the alongshore flow (again, the 130 m mooring is somewhat of an exception to this, and this is in large part due to the eddy in late June).

[24] A consistent problem in prior models of this region, regardless of their level of sophistication, is their tendency to under-predict the poleward flow that can occur at the relaxation of the equatorward winds. *Kaplan et al.* [2005] show an HF radar-derived map of the surface current associated with zero alongshore wind stress (e.g., during relaxation events) calculated from a linear regression of winds to currents using May to December 2001 data. They find a shoreward intensified poleward relaxation response inshore of the 130 m isobath, weak poleward relaxation at the 130 m isobath, and equatorward flows during relaxation offshore of this isobath. HF radar maps of the surface currents tend to show onshore flow from the outer to midshelf during relaxation, with more poleward flows inshore [cf. *Winant et al.*, 1987]. The base model accurately represents the relaxation events (Figures 2 and 4), though it underestimates poleward relaxation tendencies at 130 m and overestimates relaxation flows at 40 m. The latter problem is reduced in higher-resolution runs, and may be a symptom of an under-resolved coastline in the standard model runs.

[25] In the model runs with spatially uniform winds or with smaller domains, the upwelling relaxation is greatly reduced or eliminated (Figures 1, 2, and 3 and Tables 1, 2, and 3). Likewise, the models of *Gan and Allen* [2002a] and *Cervantes and Allen* [2006], which are also forced with spatially uniform winds, underestimate poleward relaxation flows near Point Reyes. Further to the north in the central CODE region *Gan and Allen* [2002a] show relaxation near the coast caused by pressure fields associated with Point Reyes. However, these relaxation flows are weak compared to observations, and are excessively trapped to the coast. In *Gan and Allen*'s [2002a] Figure 10, the modeled surface relaxation flows at the 60 and 90 m isobath moorings are about half to a third of those observed. The observed surface relaxation flows at these two isobaths are of roughly equal magnitude, while in their model the nearshore flow is stronger [see also *Gan and Allen*, 2002a, Figure 4].

[26] In common with other models of this region [*Gan and Allen*, 2002a; *Cervantes and Allen*, 2006], the base model does much less well at predicting the temperature evolution. While the model predicts when the surface water will warm and the deep water will cool (Figure 5), the base model becomes much too cold over the entire water column.

Table 3. Model and Current Meter Statistics for the Depth-Averaged Alongshore Flow at 130 m[a]

Data Source	Mean (cm s^{-1})	SD (cm s^{-1})	R
Large domain/full variability	−15.8	9.32	0.49
Large domain/uniform topography	−12.3	8.5	0.74
Large domain/uniform winds	−8.8	6.1	0.57
Large domain/no baroclinicity	−5.9	4.9	0.67
Medium domain	−7.5	7.6	0.12
Small domain	−15.1	10.7	0.55
Large domain/MM5 winds	−13.1	6.41	0.21
Large domain/meridional isopycnal tilt and CUC	−8.75	6.13	0.58
Current meter	−9.1	8.9	

[a]The Pearson correlation coefficient R is significant at the 95% level when $R \geq 0.36$.

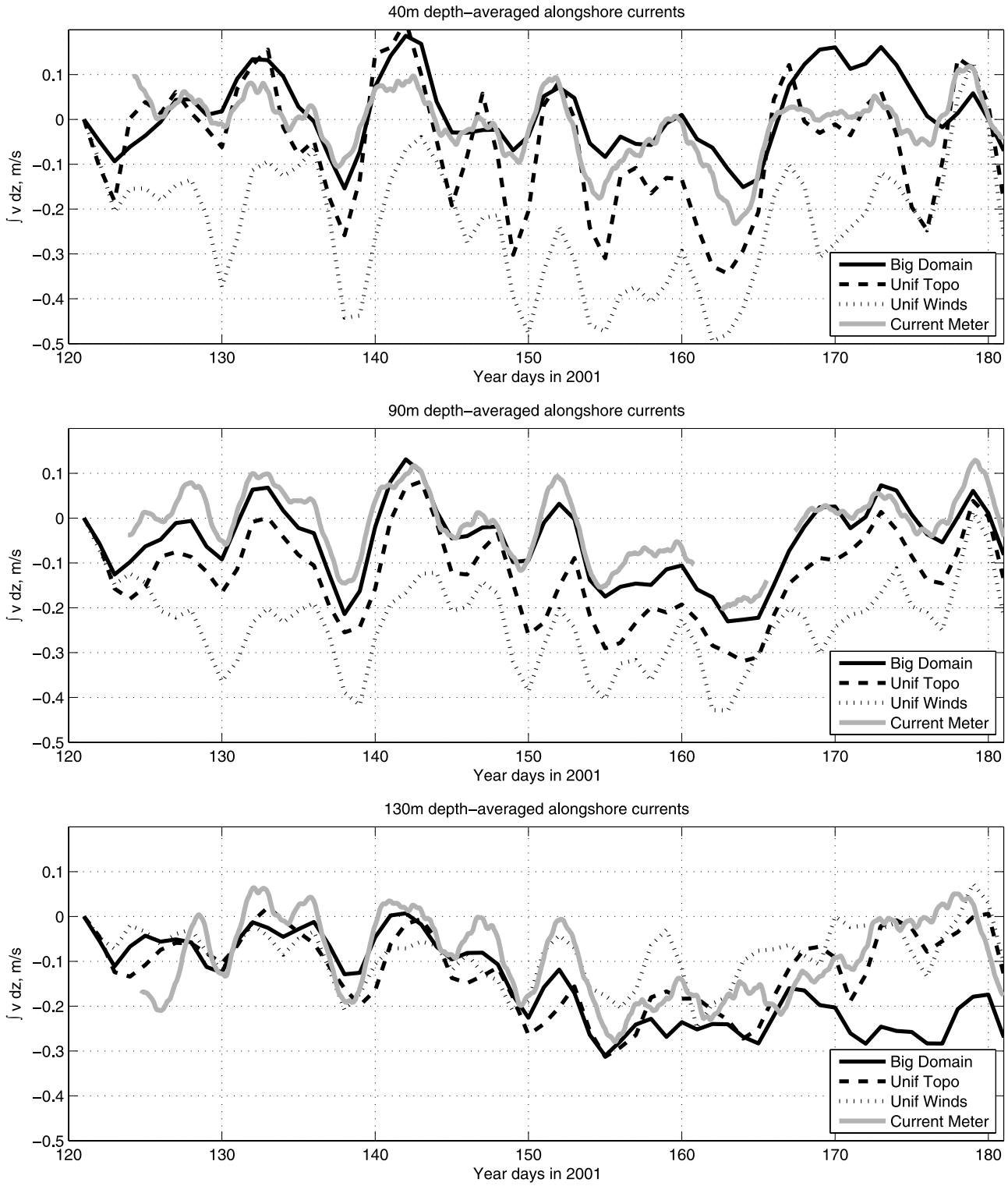

Figure 2. (top) Depth-averaged alongshore currents at the 40 m central mooring from current meters, the model with full COAMPS winds, a model with spatially uniform winds taken from the COAMPS model at the location of the central mooring, and the model with alongshore uniform bathymetry. (middle) Same as Figure 2 (top), but at the 90 m mooring. (bottom) Same as Figure 2 (top), but at the 130 m mooring. Note that for the runs with uniform bathymetry, time series are formed from currents on the appropriate isobath, not at the location of the moorings.

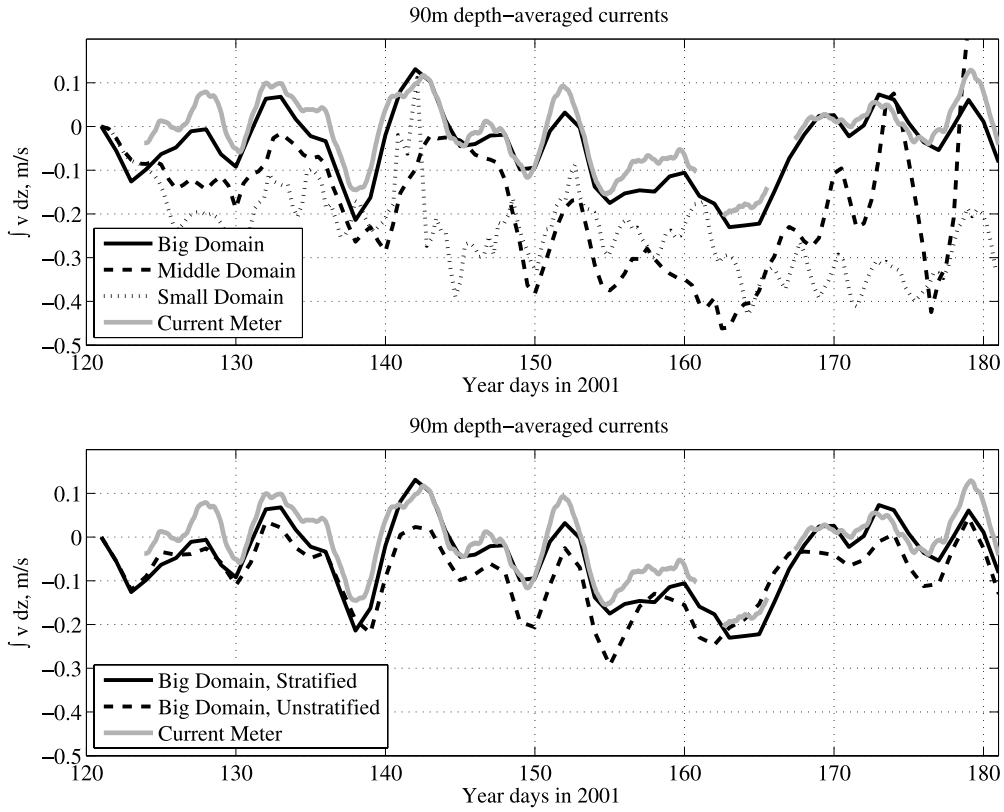

Figure 3. (top) Depth-averaged alongshore flow on the 90 m isobath for three model runs in the large, medium, and small model domains. (bottom) Depth-averaged alongshore flow on the 90 m isobath for a model in the large domain that includes and does not include baroclinic dynamics. The light gray line in Figures 3 (top) and 3 (bottom) is the depth-averaged subinertial alongshore current from the WEST observations.

Some of the error in surface temperature occurs because the model is forced with a fixed observational heat flux, and does not include the feedback between cooler surface temperatures and increased surface heat flux. However, the estimated magnitude of this error is much less than the observed temperature discrepancy, and is limited to the surface waters. The reason for the excess cooling in the model runs is discussed below.

[27] None of the models forced with only winds and surface heat flux produced a California undercurrent (CUC) that is even close to that observed [e.g., *Pierce et al.*, 2000]. This strongly suggests that the dynamics responsible for the CUC operate on scales larger than the model domains. In some runs described below, a CUC will be inserted into some model runs by either changing the initial density field of the model or by introducing a CUC through the southern boundary of the model.

[28] In the next several sections, the dynamics of the wind-driven flows in the WEST/CODE region, both modeled and observed, will be examined with the aid of the various models described above, and with the help of prior modeling efforts.

4. Effect of Spatially Variable Winds

[29] Prior efforts have found a strong relationship between winds to the south of Point Reyes and the alongshore flow there. *Denbo and Allen* [1987] found an empirical link between the remote winds and local currents, while *Chapman* [1987] used a longwave CTW model to show that much of the response was consistent with phase speeds from low-mode CTW theory. Both found that most of the remotely forced response was driven by winds just north of Monterey Bay, though there is some forcing from the region between Monterey Bay and Point Conception. The winds in these regions of remote forcing are much weaker than, but highly correlated with, the winds at Point Reyes (e.g., Figure 6, in which the correlation between winds north of Monterey and at Point Reyes is greater than 0.75).

[30] As *Gan and Allen* [2002a] point out, we would expect the flows forced by spatially varying winds to be strongly correlated to, but weaker than, the flows which would be forced by a wind which was uniform everywhere at values appropriate to the CODE region or Point Reyes. In particular, we would expect ocean models forced with realistic spatially varying winds to have reduced alongshore velocities at Point Reyes relative to models forced with spatially uniform winds representative of the winds at Point Reyes. We would also expect the alongshore flows to become weaker toward the south. This is confirmed by the model results on the 40 and 90 m isobaths, in which the mean and standard deviations of the models forced with spatially uniform winds are much larger than either the observations or the results in models forced with spatially varying winds (Figure 2 and Tables 1, 2, and 3).

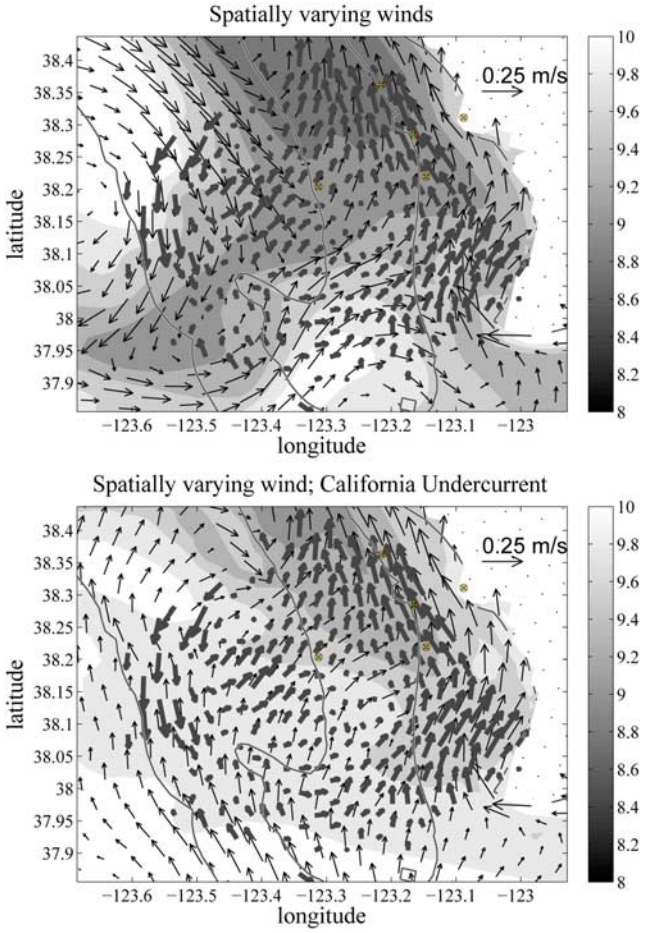

Figure 4. (top) Surface currents and temperatures at 2 m depth from the full domain model forced with spatially variable COAMPS winds from 21 May in the numerical model (thin black arrows) and the average Coastal Ocean Dynamics Applications Radar (CODAR) surface currents for 24 h around the same time (thick gray arrows). (bottom) Same as Figure 4 (top), but for the model run which includes a California undercurrent forced by inflow through the southern boundary. Bathymetry is shown at 40, 90, 130, and 1200 m. CODAR data is courtesy of *Kaplan et al.* [2005], and it has been subinertially filtered.

[31] The strength of upwelling of water from depth, and the cooling of the surface waters, should also be reduced at and south of Point Reyes by the spatially variable winds. This occurs for several reasons. The reduced alongshore currents reduce the frictional alongshore bottom stress, reducing the onshore transport of cold water in the bottom boundary layer. Furthermore, when the upwelling favorable winds increase in the direction of CTW propagation, the offshore transport of water in the surface Ekman layer is in part balanced by the convergence of the alongshore flow and the onshore transport driven at all depths by the alongshore barotropic pressure gradient, both mechanisms which would tend to reduce the transport of deeper and colder water to the surface [*Winant*, 1979; *Csanady*, 1978].

[32] To focus on the effect of spatially variable winds alone, Figure 7 shows the depth-averaged currents and 5 m temperatures after 17 days for a model forced with spatially varying winds from the May–June 2001 average COAMPS winds, and for a model forced with spatially uniform winds whose strength is equal to the COAMPS May/June mean winds at the 90 m Central WEST mooring. The spatially varying winds produce weaker alongshore currents, which drive a weaker upwelling response and warmer temperatures near the surface, and indeed throughout the water column. While this weakening is most pronounced in the southern part of the domain, it extends well north of the WEST site to locations where the local winds are even stronger than those at Point Reyes. Associated with the weaker alongshore flows is an alongshore temperature gradient, with colder and denser water to the north. This is consistent with *Gan and Allen*'s [2002a] attribution of a significant part of the overprediction of alongshore currents in their model to their use of a spatially uniform wind forcing. Likewise, the smaller domain models shown in Figure 1 have overly strong currents because they do not fully encompass the region of weaker winds.

[33] In the model run with uniform winds, there is also overly strong flow near the shore because the uniform winds do not capture the reduced wind stress near the shore. This has recently been numerically modeled by *Kuebel-Cervantes and Dever* [2006] and analyzed by *Lopez-Mariscal and Clarke* [1993].

[34] The effects of spatially varying winds are not, however, confined to the strength of the current fluctuations they drive. In the runs made with spatially uniform winds, upwelling relaxation flows are inhibited and the depth-averaged flows near Point Reyes at the 40 and 90 m isobaths do not show current reversals when the winds weaken (Figures 2 and 8). The dynamics linking spatial variation in wind strength and upwelling relaxation will be described below.

5. Effect of Alongshore Variation in the Bathymetry

[35] Not all of the reduction in equatorward flow relative to the prior modeling is due to the weakening of the winds to the south. *Pringle* [2002] has shown in a simple steady model that neglects stratification that when a shelf widens in the direction of CTW propagation the along-shelf flow is weakened and upwelling is reduced, and that when it narrows, the converse occurs. *Pringle* [2002] calculates that relative to the flow over an alongshore-uniform shelf, alongshore flows and upwelling are reduced between Monterey Bay and Point Reyes, and are enhanced where the shelf narrows to the north in the CODE region and toward Point Arena.

[36] This reduction can be seen in the difference between model runs made with realistic and alongshore uniform bathymetry. In Figure 7, where the shelf narrows toward Monterey Bay the alongshore flow is reduced near and to the north of the Bay, but when the shelf is set to a constant width the flow is more nearly the same magnitude along the coast. Where the alongshore flow is weaker, the upwelling of cold water is weaker, as predicted by *Pringle* [2002]. This leads to an alongshore gradient in density with denser water to the north.

[37] Farther to the north, around Point Reyes, there is little change in the magnitude of the alongshore current

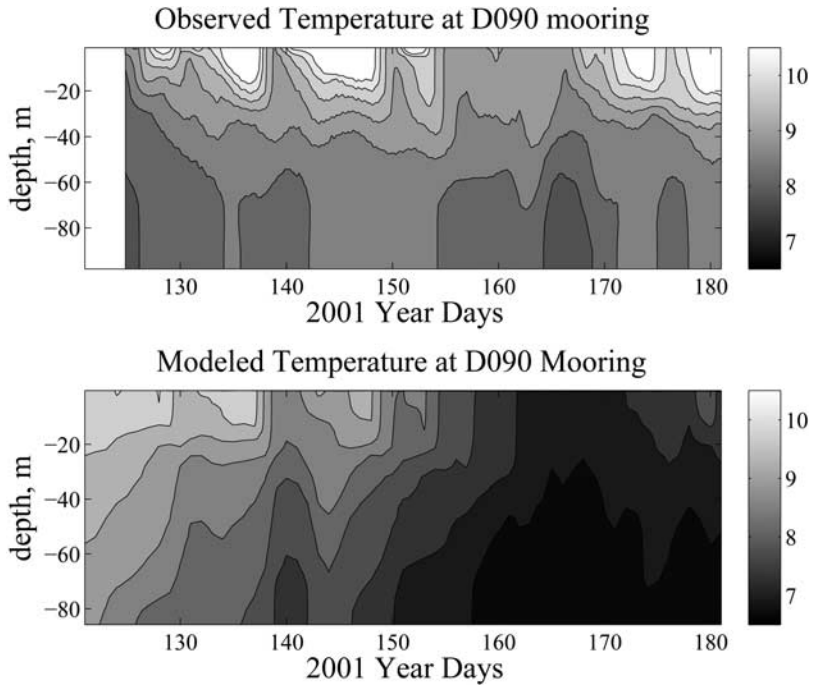

Figure 5. The temperature at the D090 mooring as a function of time and depth for (top) the D090 mooring and (bottom) the full model with large domain, alongshore varying bathymetry, and spatially and temporally varying COAMPS winds. The mooring data has been low-pass filtered in the same way as the winds used to force the model have been.

fluctuations between the alongshore-uniform bathymetry and the actual bathymetry. However, the mean flow is more equatorward in the model runs with uniform bathymetry (Tables 1, 2, and 3 and Figure 2), suggesting that alongshore uniform bathymetry reduces the upwelling relaxation response.

[38] The effect of changes in shelf width is much less in models that have either a relatively short alongshore extent or are alongshore periodic. The alongshore periodic models of *Gan and Allen* [2002a] and *Cervantes and Allen* [2006] remove much of the alongshore variation in shelf width in order to allow the northern and southern cross-shelf boundaries to join up. In these models the extreme narrowing of the shelf near Monterey Bay is eliminated in order to allow the shelf there to be of the same width as the shelf north of Point Arena. The smallest domain model shown in Figure 1

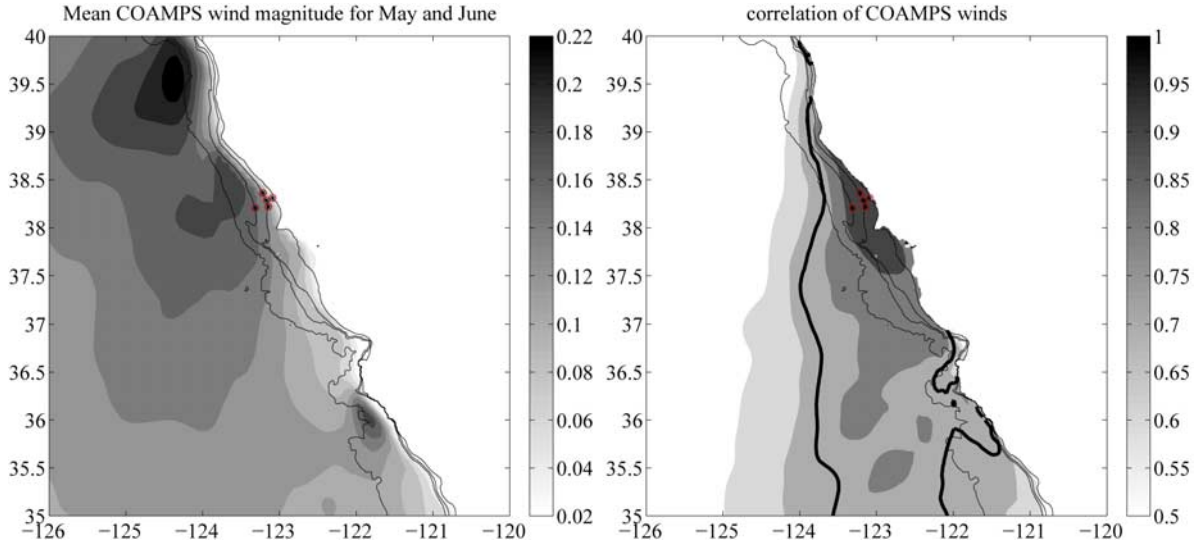

Figure 6. (left) The magnitude of the COAMPS wind stress averaged from May to June of 2001. Bathymetry is shown at 40, 90, 130, and 1200 m. (right) The vector correlations between the model winds at the location of the 90 m central WEST mooring and the winds elsewhere. The thick black contour encloses the region where the correlation is greater than 0.75.

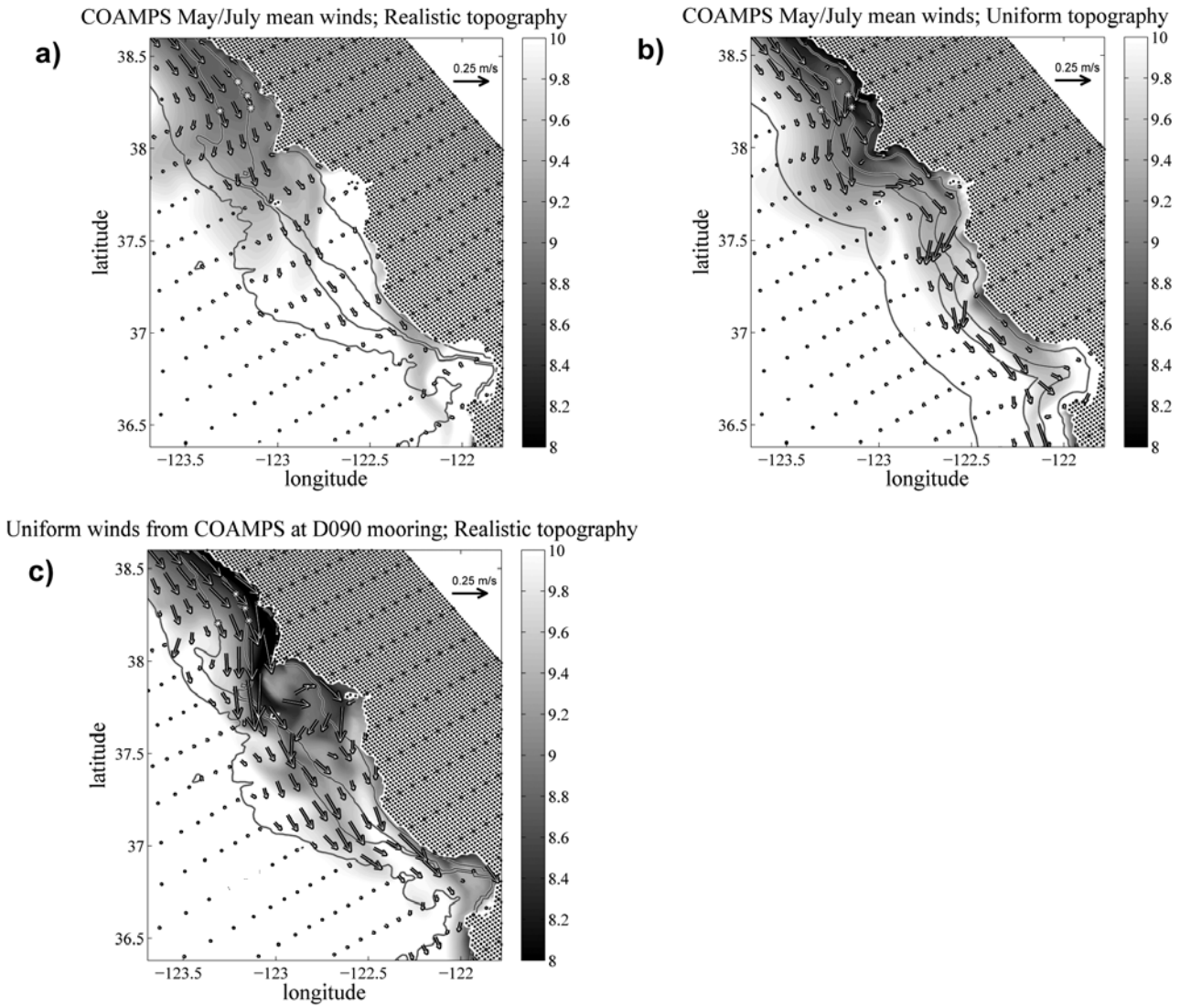

Figure 7. Depth-averaged alongshore currents and surface temperature from three models after each was forced with a temporally steady wind for 17 days. (a) The full spatial structure of the COAMPS May–June 2001 average winds is used. (b) The same winds are used, but an alongshore-uniform bathymetry is used. (c) A spatially uniform wind is used, and its strength is the strength of the May–June 2001 COAMPS average wind at the central 90 m WEST mooring. Bathymetry is shown at 40, 90, 130, and 1200 m.

also does not include the full extent of the shelf narrowing near Monterey Bay. These deficiencies contribute to excessively equatorward flows in both the small domain model and the alongshore-periodic models.

6. Interactions Between Alongshore Variation and the Density Field: The Origin of Upwelling Relaxation

[39] Our results suggest that both the alongshore variation of winds and bathymetry lead to a weakening of the alongshore flow between Monterey Bay and Point Arena. However, they do not explain why, when the winds cease, there is a strong poleward flow over much of the shelf. The idealized theories invoked above to explain the alongshore gradients in alongshore flow are wind forced, and when the winds stop, the flow predicted by these theories will cease in a relatively short period of time. However, we see in both the data and the model response (Figures 2 and 4 and *Kaplan et al.* [2005] and *Winant et al.* [1987]) that upon the relaxation of winds the flows do not come to halt, but become poleward and onshore. The onshore flows are stronger toward the surface and on the outer shelf and are balanced both by transport in the bottom boundary layer and divergence of the alongshore flow. The poleward flows are strongest in the shallower waters, and become progressively weaker offshore, until at midshelf the relaxation flows are only weakly poleward and offshore of that mooring they are equatorward.

[40] The poleward flow during relaxation events is not primarily driven by poleward wind reversals. To show this, several model configurations are forced with temporally uniform winds for 20 days, and then this wind relaxes to zero over 1 day (Figure 8). In one model run, the spatial

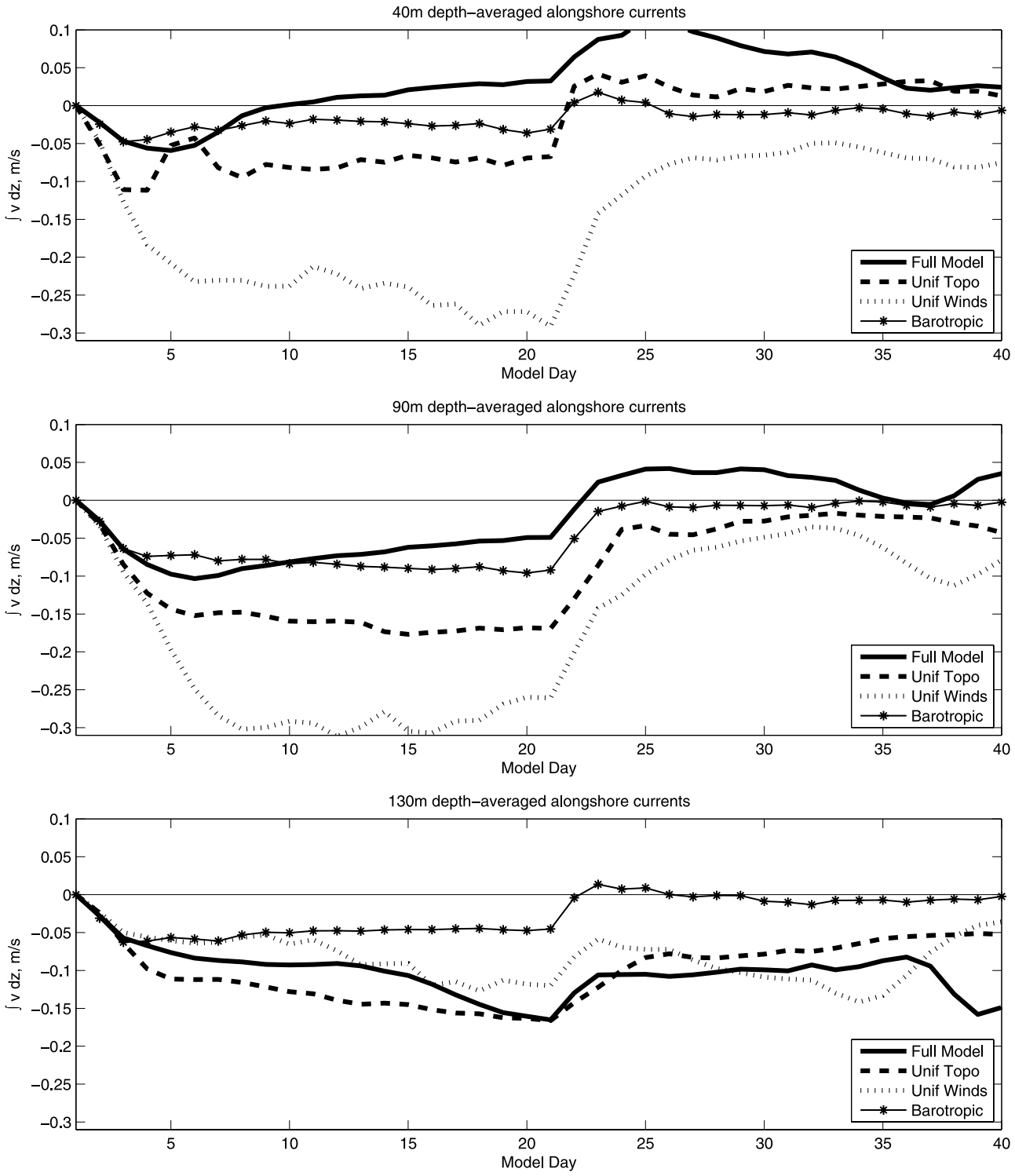

Figure 8. Alongshore depth-averaged currents in model runs made with idealized winds that are steady for 20 days and then relax to zero over 1 day. (top) From the 40 m mooring location in the full model with the spatial patterns of COAMPS winds from the May–June 2001 average winds; a model with spatially uniform winds taken from the above COAMPS winds at the location of the central mooring; a model with alongshore-uniform bathymetry and the spatially varying COAMPS pattern winds; and the model with spatially varying winds, alongshore varying bathymetry, and with uniform density (labeled "barotropic"). (middle) Same as Figure 8 (top), but at the 90 m mooring. (bottom) Same as Figure 8 (top), but at the 130 m mooring. Note that for the runs with uniform bathymetry, time series are formed from currents on the appropriate isobath, not at the location of the moorings.

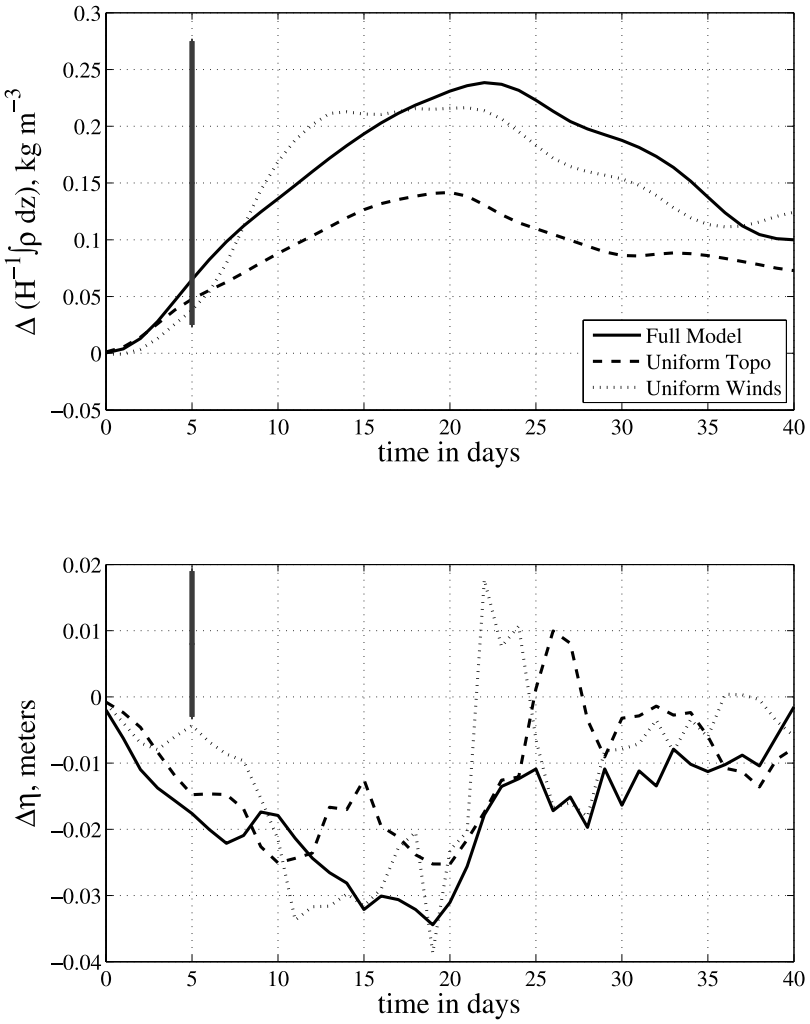

Figure 9. (top) The difference between the depth-averaged density on the 90 m isobath at 38.5 ± 0.1° and 37.0 ± 0.1° in models forced with steady winds which cease after 21 days, as in Figures 7 and 8. (bottom) The difference between the free surface elevation on the 90 m isobath at the same latitudes. A positive difference indicates that the value is greater to the north. The magnitude of the density and sea surface height differences can be compared by noting that a depth-averaged density difference of 0.25 kg m^{-3} (shown as a vertical bar in Figure 9 (top)) leads to the same change in bottom pressure as a 0.022 m change in sea surface height in 90 m deep water (shown as a vertical bar in Figure 9 (bottom)).

pattern and magnitude of the winds comes from the May–June 2001 mean of the COAMPS winds, and realistic bathymetry is used. In the second, the same winds are used, but the shelf width does not vary in the alongshore direction. In the third model run, the full bathymetry is used, but the winds are spatially uniform and their intensity is appropriate to the mean winds at the location of the central 90 m mooring. In the fourth model, spatially variable winds and bathymetry are used, but the temperature and salinity do not affect the model density, i.e., all baroclinic dynamics are removed. In baroclinic model runs with the full spatial structure of winds and bathymetry, there is a strong poleward flow after the winds cease at the 90 m and 40 m moorings, and this poleward flow slowly decays over roughly two weeks. In the other model runs, the relaxation flows are not present or are weaker and in shallower water. In particular, in the runs without baroclinic dynamics, flow comes nearly to a halt when the wind halts. To understand the upwelling relaxation flow, we must consider the interactions of alongshore variation in forcing and bathymetry with the effects of baroclinicity on the alongshore flows.

[41] In an ocean with little alongshore variation in winds and bathymetry, the baroclinic flows driven by upwelling winds are also in the downwind direction [e.g., *Austin and Lentz*, 2002]. Upwelling winds form an upwelling front, which on this coast will drive an equatorward flow. When the wind ceases, that upwelling front will tend to remain offshore, at least in idealized models of alongshore uniform shelves, and will continue to cause an equatorward flow until the front is dissipated by some mechanism [*Austin and Lentz*, 2002]. This is seen in our idealized wind experiments on the 130 m isobath, in which all models that include density variation show equatorward flow after the wind ceases, while the flow in the model that does not include

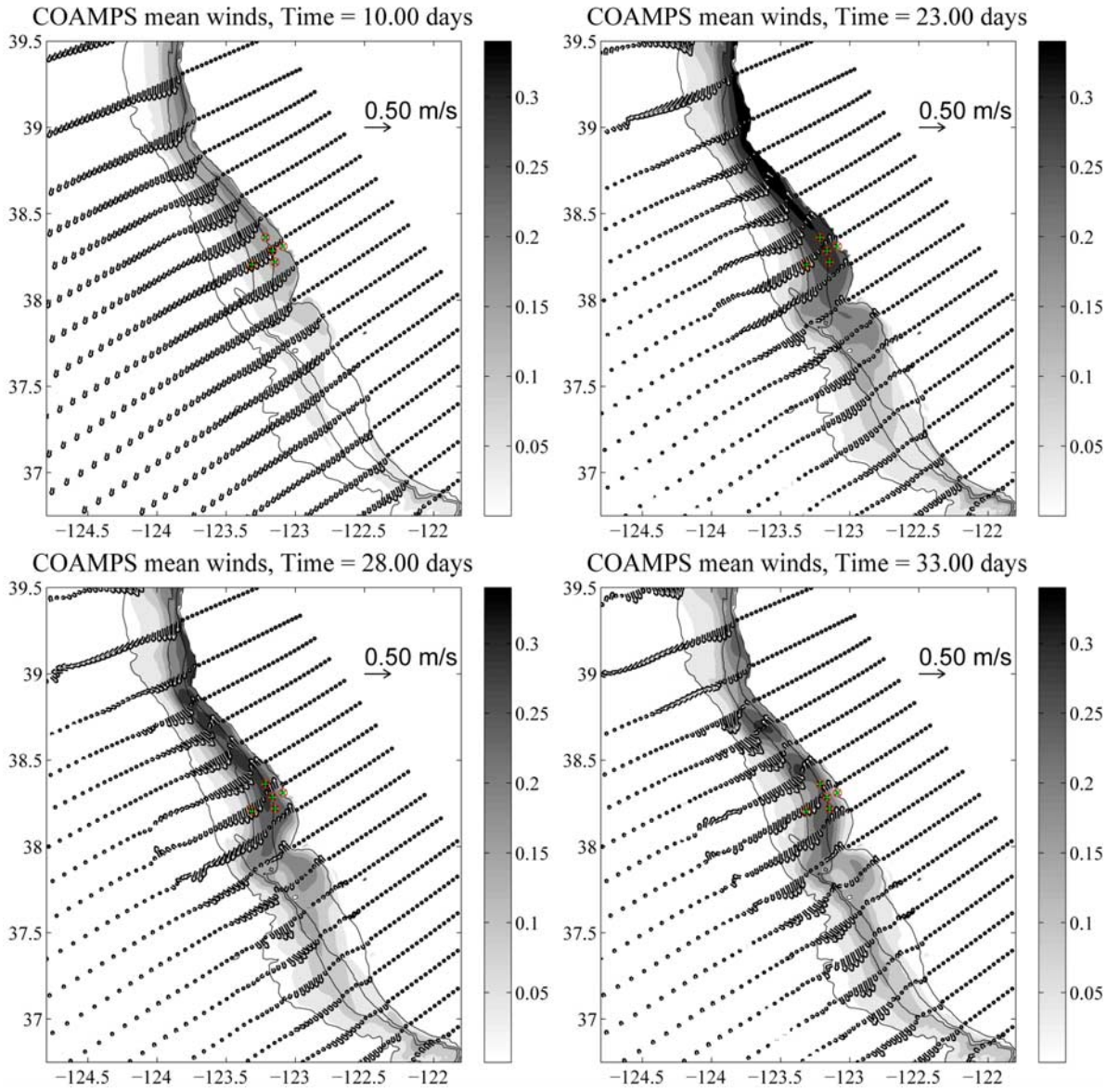

Figure 10. The velocity at 5 m depth (arrows) and the depth-averaged density anomaly relative to the initial depth-averaged density in kg m^{-3} (shading). The model run was forced with a temporally steady, spatially varying wind for 20 days, after which the wind relaxes to zero over 1 day. The winds are the May–June 2001 average COAMPS winds. Plots are shown for days 10, 23, 28, and 33.

density variation comes to a halt when the wind ceases. This equatorward flow is consistent with thermal wind and the observed cross-shelf density gradients in the model (not shown).

[42] However, in model runs with alongshore variations in the wind, the bathymetry, or both, the alongshore gradient in the strength of upwelling (Figure 7) generates alongshore gradients in the depth-averaged density along an isobath (Figures 9 and 10). This alongshore gradient, from less dense in the south to more dense to the north, is associated with a sea surface height gradient with higher sea surface to the south, and lower to the north, for reasons given below. In the model runs, the surface height field and the density field coevolve while the wind blows and, when the winds stop, there is a rapid adjustment that leads to the ejection of a low-mode CTW from the region. The dynamics described below are attained on either the frictional decay scale [*Dever*, 1997] or the time it takes a low-mode CTW to transit the region, whichever is longer. Subsequently the coevolution of the density and surface elevation is governed by the advection of density, which we have assumed to occur on a timescale long compared to adjustment of the sea surface height to the density field. The alongshore surface pressure gradient leads to a poleward flow. In the model with full alongshore wind and bathymetric variation, the tendency for the alongshore density gradient to lead to poleward flows overcomes the tendency of the cross-shore density gradient to force equatorward flows after the winds have ceased. At the shallowest mooring, poleward flow begins even before the cessation of the wind (Figure 8). The

poleward relaxation flows increase in strength to the north, and are largely limited to the inner two thirds of the shelf in both the models and observations (Figure 4).

[43] It may seem odd that an alongshore density gradient will drive an alongshore flow, i.e., toward, the denser water. To illustrate qualitatively why this might be so, we follow *Vennell and Malanotte-Rizzoli* [1987], hereafter VMR, and examine the linear vorticity equation in the case that there is a depth uniform density anomaly $\epsilon = (\rho - \rho_0)\,\rho_0^{-1}$, where ρ is the local density and ρ_0 is the mean density (Figure 10 gives $\rho_0\epsilon$ for a model forced with spatially varying winds). For this qualitative analysis, let us assume that ϵ only varies in the alongshore direction, so that $\epsilon_x = \epsilon_z = 0$, and let us assume a shelf of alongshore uniform bathymetry. We are interested in times long enough that the flow has reached a nearly steady state, but not so long that the along-shelf or vertical advection of density has significantly altered the density field. We also assume the shelf is wide compared to the internal radius of deformation. (For background, see VMR and *Pringle* [2002].) For realistic parameter ranges appropriate to Point Reyes the weakest assumption is the neglect of density advection, for while the density driven flow in the model sets up in 1 day or two (Figure 8), over a timescale of 5 to 10 days the advection of density significantly modifies the density field (Figures 9 and 10). However, the numerical model results are qualitatively similar to those described below. The steady depth-integrated momentum and continuity equations under these assumptions are

$$-fV = -gh\eta_x - ru^b \tag{1a}$$

$$fU = -gh\eta_y - \frac{gh^2}{2r}\epsilon_y - rv^b \tag{1b}$$

$$U_x + V_y = 0 \tag{1c}$$

where x is the cross-shelf direction, U and V are the depth-integrated velocities, u^b and v^b are the velocity near the bottom, and r is a linear coefficient of bottom friction. If we assume the alongshore length scale is much greater than the cross-shore length scale, the friction in the cross-shore momentum balance (ru^b) can be neglected (VMR). Assuming that friction is proportional to the near bottom geostrophic flow, and assuming a thin bottom boundary layer (some empirical justification for assuming geostrophy near the bottom in these regions can be found in the paper by *Lentz and Trowbridge* [2001]), we can say

$$v^b = \frac{g}{f}\eta_x \tag{2}$$

where ϵ_x is assumed small as above. Cross differentiation of (1a) and (1b) and eliminating velocity leads to a steady linear vorticity balance of

$$\eta_y + \frac{r}{h_x f}\eta_{xx} = -h\epsilon_y \tag{3}$$

where h is the water depth and, for the west coast, $h_x < 0$. Assuming that h becomes vanishingly small at the coast, the coastal boundary condition of $U = 0$ becomes

$$\eta_x = 0 \quad @ \quad x = 0. \tag{4}$$

[44] This is the familiar "arrested topographic wave" (ATW) equation system of *Csanady* [1978] and others, modified to include the effects of density gradients. It is also similar to *Huthnance*'s [1984] JEBAR solutions, in the depth-averaged longwave limit.

[45] As has been pointed out by many (and in this context by VMR), equation (5) resembles a heat equation, and on a Northern Hemisphere west coast should be integrated along-isobaths northward, in the direction of long coastal trapped wave propagation. The effects of any forcing will be felt only to the north of the forcing (thus any flows caused by the along-isobath density gradients will be felt at and to the north of the density gradient).

[46] Let us assume that the ocean is motionless and uniform to the south of $y = 0$, but that to the north of that point there exists a uniform alongshore density gradient and a bottom which slopes linearly offshore ($h = -\alpha x$, $\alpha > 0$). The particular solution to equation (5) is then

$$\eta = -h\epsilon_y y \tag{5}$$

which says that if the water becomes denser to the north ($\epsilon_y > 0$) the sea level will decrease to the north. This particular solution satisfies equation (5), but not the coastal boundary condition. As one moves northward, the effect of coastal boundary condition will diffuse onto the shelf, as suggested by equation (5) and described by VMR, and equation (7) will be valid only further offshore. Nonetheless, at locations close enough to $y = 0$ and far enough offshore that they are not affected by the coastal BC, the northward decrease in sea level will drive an onshore geostrophic flow balanced by the cross-shelf thermal wind flow such that the geostrophic flow at the bottom is zero and becomes stronger toward the surface (to see this, note that the alongshore change of η is just enough that the depth integrated mass is uniform along an isobath).

[47] However, the depth-averaged cross-shelf transport cannot persist across the shelf because of the coastal boundary condition. Because the effects of the forcing are only felt to the north of the forcing, the onshore flow driven by the northward density gradient must turn north at the coast and flow northward toward the denser water. It is straightforward to show that on other shelves in other hemispheres the result is the same (the alongshore flow driven by a large-scale alongshore density gradient will tend to be toward the denser water). Another way to understand this result is to note that the surface elevation gradient causes a poleward force on the water column. As with a poleward wind forcing, this drives a poleward flow when there is a coastal boundary [*Lentz and Trowbridge*, 2001].

[48] To estimate the magnitude of the flow caused by the alongshore gradient in density, we use a result from VMR and *Pringle* [2002]. They find that along a shelf of uniform width and uniform offshore slope such as described above,

the coastal boundary conditions affect the flow on the isobath at depth h a distance

$$L^x = \frac{1}{2}\frac{f}{r}\frac{h^2}{\alpha} \tag{6}$$

to the north, on this coast, of the beginning of the density gradient. The geostrophic onshore transport between the start of the density gradient and the point L^x downstream implied by equation (7), $\frac{gH^2}{2f}\epsilon_y L^x$, must be balanced by an alongshore flow between the coast and the h isobath. The cross-sectional area of the shelf inshore of h is $\frac{h^2}{2\alpha}$, so the mean flow speed of the alongshore current a distance L^x from the start of the density gradient will then scale as

$$v_{ave} = \frac{gh^2}{2r}\epsilon_y. \tag{7}$$

In the model, the along-isobath density gradient is strong between Monterey Bay to just south of Point Arena (Figure 10), and becomes significantly weaker offshore of the 90 m isobath. This suggests that the upwelling relaxation is primarily driven by the along-isobath density gradients in this region. For the density gradient in the large domain model forced by spatially varying mean May/June 2001 winds on the 40 m and 90 m isobaths of about 1.5×10^{-6} kg m^{-4} and a typical r of 3×10^{-4} m s^{-1}, this suggests an alongshore velocity of about 5 cm s^{-1} at 40 m depth and 20 cm s^{-1} at 90 m depth. The 40 m speed estimate is somewhat low compared to the model, while the 90 m estimate is somewhat large, but both are of the right order of magnitude. The overestimate of the 90 m speed occurs for several reasons. Primarily, L^x from above at 90 m is about 250 km, which is greater than the distance from Monterey Bay to Point Reyes. Thus the alongshore flow on the 90 m isobath at Point Reyes has not fully adjusted to the alongshore pressure gradient. Also important is the widening of the shelf north of Monterey Bay, which tends to reduce the midshelf alongshore flow at Point Reyes [*Pringle*, 2002], and the upwelled isopycnals on the shelf, which tend to drive equatorward flows. Even if these other effects were accounted for, it must be born in mind that this is a qualitative result, for advection will quickly alter the density field (Figure 10 and *Shaw and Csanady* [1983]).

[49] Nonetheless, the phenomenology of the flow is straightforward: alongshore density gradients will tend to drive cross-shelf flows and flows in the direction of the denser water, both at the location of the density gradient and downwave of them. On this coast, a poleward density gradient causes surface-intensified onshore and poleward flows, consistent with the observed poleward flows and upwelling relaxation response (Figure 4). The onshore flows will dominate on the outer part of the shelf, and the poleward flows will dominate closer to the coast. As one moves poleward, the poleward flow will dominate over more of the shelf. With time, the circulation driven by these flows will tend to reduce the alongshore density gradient. In Figure 10, the density anomaly can be seen to be greatly reduced 10 days after the cessation of the wind, both by the poleward advection of less dense water near the coast and by the downwelling circulation caused by the poleward pressure gradient. The poleward flow near the coast moves warmer water around Point Reyes, as observed by *Send et al.* [1987] and *Wing et al.* [1995] (Figures 10 and 11).

[50] The analysis above suggest that upwelling relaxation flow is an emergent property of the Monterey Bay–Point Reyes–Point Arena upwelling system, driven by the alongshore variation in bathymetry and winds. Alongshore variability in the shelf width and the strength of the winds leads to alongshore density gradients that drive the upwelling relaxation circulation. When the winds relax, the density driven flows dominate, leading to the observed relaxation circulation. Prior discussions of upwelling relaxation have often attributed the poleward relaxation flows to large-scale pressure gradients established by the gyre-scale circulation [*Gan and Allen*, 2002a; *Send et al.*, 1987], though *Oey* [1999] did suggest that spatial variation in the wind might cause some poleward flows. However, the model results presented above suggest that, at least on the shelf in this region, much of the relaxation is due to dynamics local to the shelf between Point Reyes and Monterey and in the regions immediately to the south.

7. Large-Scale Controls on Shelf Temperature During Upwelling

[51] The above results present a conundrum. Shelf currents are well reproduced by the base case model, suggesting that the shelf dynamics have been properly captured, but the waters on the shelf become much too cold, suggesting they have been drawn from an excessive depth. This is confirmed by a comparison with the data. In both the model and observations, near bottom temperature on the shelf reaches a steady state in early June, despite the continuation of strong upwelling-favorable winds for the entire month. *Roughan et al.* [2006] computes a summer 2001 mean hydrography and finds that the isopycnals from 200 m to 160 m depth are roughly flat across the slope, and the temperature of the upwelled water at the base of the central 90 m mooring in June, about 8.25°C, is consistent with water being upwelled from about 150 m depth onto the shelf. By contrast, in the base model runs, the bottom temperature for most of June 2001 is about 6.75°C, and is consistent with water being upwelled from 300 m depth on the slope. (Because the base model was initialized with horizontally uniform temperature and salinity to match prior work, and because runs described below will alter the initial vertical temperature distributions, we will discuss the depth from which water is upwelled and not just the temperature of the water on the shelf.)

[52] So what controls the depth from which water is drawn? The deep water is drawn to the shelf from the slope so we must focus on mechanisms of upwelling that are active there. In a nearly two-dimensional subinertial system, the cross-isobath transport at each depth must be driven by an along-isobath forcing at that depth. The along-isobath wind forcing drives a cross-shelf Ekman transport that must be balanced by flows forced by along-isobath bottom stress, along-isobath pressure gradients, or the divergence of the cross-shelf advection of along-shelf momentum [*Lentz and Chapman*, 2004]. It seems unlikely that a model/data discrepancy in bottom stress over the slope is the answer

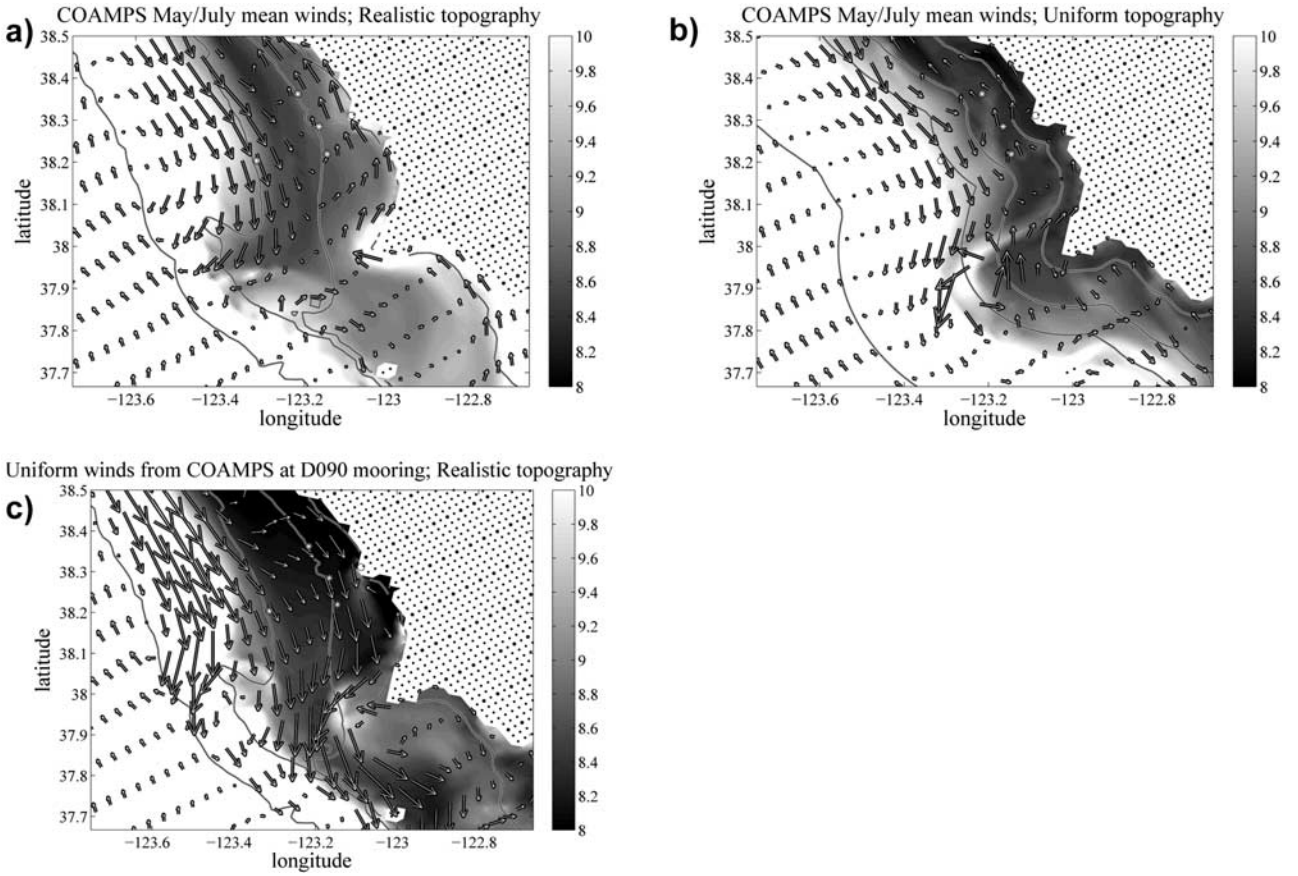

Figure 11. Depth-averaged alongshore currents and surface temperature from three models, each forced with a temporally steady wind for 20 days, after which the wind relaxes to zero over 1 day. The model output is shown 5 days after the winds have ceased. (a) The full spatial structure of the COAMPS May–June average winds is used. (b) The same winds are used, but an alongshore-uniform bathymetry is used. (c) A spatially uniform wind is used, and its strength is the strength of the May–June COAMPS average winds at the central 90 m WEST mooring. Bathymetry is shown at 40, 90, 130, and 1200 m.

(comparisons of near bottom currents between the base case model and ADCP observations find substantial agreement on the slope). In both the model and the summer observations of *Pierce et al.* [2000] the near bottom currents on the slope are much too small to produce an along-shelf stress comparable to the alongshore wind stress for any reasonable value of the bottom friction coefficient. *Pierce et al.* [2000] finds that the along-shelf near-bottom velocities are generally less than 10 cm s^{-1} in each section, and less than 5 cm s^{-1} in an alongshore average.

[53] Errors in the model's calculation of the divergence of the cross-shelf advection of along-shelf momentum over the shelf could lead to errors in upwelling over the slope. In observations of the slope, there is a persistent California Under Current (CUC), a poleward undercurrent with a peak magnitude of about 20 cm s^{-1} and a cross-shelf extent of about 20 km centered between 150 and 275 m depth over the slope [*Pierce et al.*, 2000]. This current is not present in the base model runs, and it might seem that the divergence of the cross-shelf advection of this poleward flow might provide a forcing which counterbalances the surface equatorward wind stress. Divergence of the cross-shelf advection of the along-shelf momentum of wind-driven flows have been found by *Lentz and Chapman* [2004] to force the upwelling return flow higher in the water column, and they found this mechanism to be more important over steeper slopes. However, a scaling of the magnitude of this term of the momentum equation, assuming that the cross-shelf transport scales as the wind-driven Ekman transport and the along-shelf flows have the scales of the CUC given above, finds that the depth-averaged magnitude of this term is 10 to 20% of the depth-averaged vertical stress divergence for a typical along-shelf wind stress of about 0.1 N m^{-2}. Hence the divergence of the cross-shelf advection of along-shelf momentum is unlikely to be a dominant term in the alongshore momentum equation. Analyses of the alongshore momentum budget in model runs support this.

[54] This leaves the along-isobath pressure gradients over the slope as a mechanism for driving cross-shelf flows that can modify the source of upwelled water to the shelf. Over the slope, an equatorward pressure gradient (e.g., a poleward pressure gradient force) will drive an onshore geostrophic flow that can be balanced by both the bottom Ekman layer transport offshore and the alongshore divergence of a poleward flow, as described above. However, when there is an upwelling favorable wind, some portion of the offshore transport in the surface Ekman transport can be balanced by the onshore geostrophic transport driven by the along-slope pressure gradient. This will reduce the importance of transport in the bottom boundary layers, and cause

the upwelled waters on the shelf to be replaced by water from a shallower depth on the shelf. A formal analysis of this can be found in the paper by *Lentz* [2008]. *Lentz and Chapman* [2004] describe how these dynamics will be altered by the cross-shelf advection of momentum.

[55] Evidence for an along-isobath pressure gradient over the slope along the west coast of North America is sparse but persuasive. A steric height anomaly along the slope is observed, with an equatorward gradient of about 5 cm between 35° and 40°N when referenced to 1000 dbar [*Reid and Mantyla*, 1976; *Hickey and Pola*, 1983] (see also N. Maximenko and P. Niiler (Mean surface circulation of the global ocean inferred from satellite altimeter and drifter data, paper presented at Fifteen Years of Progress in Radar Altimetry, European Space Agency, Venice, Italy, 2006), who find similar results from a combination of altimeter and hydrographic data). Observations of a continuous poleward undercurrent along the slope [*Pierce et al.*, 2000] are consistent with this poleward pressure gradient [*Werner and Hickey*, 1983; *Neshyba et al.*, 1989; *McCreary*, 1981]. The origin of the along-slope pressure gradient is poorly understood, and has been considerably debated (see citations above and *McCreary et al.* [1991]). There is some evidence that the along-slope pressure gradient is linked to regional winds: Using 24 years of coastal tide gauge data in this region, *Enfield and Allen* [1980] found that on timescales greater than a month or two, the alongshore pressure gradient is significantly (but not strongly) correlated with the regional alongshore wind such that the cross-shelf barotropic geostrophic flow over the top 100 to 300 m would balance the cross-shelf Ekman transport. The dynamics of this along-slope pressure gradient must involve spatial scales larger than the large model domain shown in Figure 1 or temporal scales longer than the two month integrations, for the undercurrent does not develop of its own accord in our model runs but does in multiyear integrations of basin-scale models of Pacific [*Garfield et al.*, 2001; *Choboter et al.*, 2002]. The offshore extent of the along-slope pressure gradient is not clear. For example, in the World Ocean Atlas of the National Oceanographic Data Center there is little alongshore isopycnal slope in the data closest to the west coast of North America [*Locarnini et al.*, 2006; *Antonov et al.*, 2006; *Garcia et al.*, 2006a, 2006b]. The climatology is computed with data gathered over a one degree or somewhat larger area, suggesting that perhaps the observed alongshore steric height anomaly does not extend very many degrees offshore. Likewise, the depth structure of the along-slope pressure gradient is also uncertain, with the core of the CUC varying greatly in depth between various observations.

[56] Given the uncertainty in the structure and dynamics of the along-slope pressure gradient, the modeling will attempt to include the undercurrent by adjusting the model forcing or initial condition to achieve a CUC that is similar to that described by *Pierce et al.* [2000] and *Noble and Ramp* [2000]. The target is a CUC with a peak magnitude of about 20 cm s^{-1} and a cross-shelf extent of about 20 km centered between 150 and 275 m depth over the slope. Because of the uncertainty in the undercurrent dynamics, the CUC will be inserted into the model in two ways. First, to emulate an undercurrent and pressure gradient that are forced by a steric height anomaly along the coast, the model was initialized with a temperature and salinity field in which the isopycnals sloped upward with increasing latitude by an amount roughly consistent with an along-slope survey conducted by *Pierce et al.* [2000], shown in their Figure 8a. At depths of 0, 100, 600, and 1400 m the isopycnals sloped upward to the north by 0, 110, 250, and 112 m per 15 degrees of latitude, with the pivot point for the isopycnals at 38.3°N so that the stratification in the Point Reyes region is nearly unchanged in the various model runs. The isopycnal slope is linearly interpolated between these depths. When this large domain model is run without any wind forcing, it quickly spins up a very realistic appearing CUC in the vicinity of Point Reyes, and the along-slope sea surface height change between 35° and 40°N of 4 cm is roughly consistent with the steric height change calculated by *Reid and Mantyla* [1976]. Invoking an along-isobath density gradient is not a complete dynamical explanation for the CUC. It does not explain how the along-slope density gradient can be maintained in the face of Rossby wave dynamics that would tend to remove the gradient and flatten the isopycnals. Even in the two month run described here, the CUC noticeably evolves as the alongshore density anomaly propagates offshore at a speed consistent with westward Rossby Wave propagation [*Clarke and Dottori*, 2008]. However, at least for the first month of these integrations, this effect is minor.

[57] A second model run was made to include the possibility that the CUC is entirely remotely forced. In this run, 2.3 Sv of water is forced into the model domain over the shelf on the southern boundary [*Noble and Ramp*, 2000; *Bray and Greengrove*, 1993]. As described by *Chapman* [1986], this flow quickly moves across the shelf and forms a poleward current over the slope. The dynamics of such a slope jet have not been well analyzed, for it first evolves as described by arrested topographic wave dynamics, but soon the advection of density, particularly in the bottom boundary layer, modifies its evolution, so that its dynamics share some similarities with those described by *Chapman* [2003]. Nonetheless, by the time the jet reaches the Point Reyes region, it has also set up in the model an along-slope surface height gradient of about 4 cm height change between 35° and 40°N. It has also set up a CUC that is similar to that reported by *Pierce et al.* [2000] and *Noble and Ramp* [2000], as shown in a model run in which there is no wind in Figure 12.

[58] An along-slope pressure gradient of great alongshore extent would be expected to influence the shelf circulation [*Middleton*, 1987]. However, the along-slope pressure gradient imposed on the model in these runs is about 2.5 times less than the along-shelf gradient created by variation in winds and bathymetry discussed in the last section (Figure 9). Further, where the shelf widens in the direction of CTW propagation and isobaths become farther apart, flow which even roughly follows isobaths will tend to weaken, as described by *Pringle* [2002]. As shown in Figure 12 and Tables 1 and 2, these alongshore pressure gradients on the slope have little impact on the shelf circulation to the north of Monterey Bay where the shelf widens, and immediately to the north of Cape Mendocino, but can be important elsewhere, for example near Point Arena. This is consistent with *Noble and Ramp* [2000], who found that along-slope pressure gradients on the slope

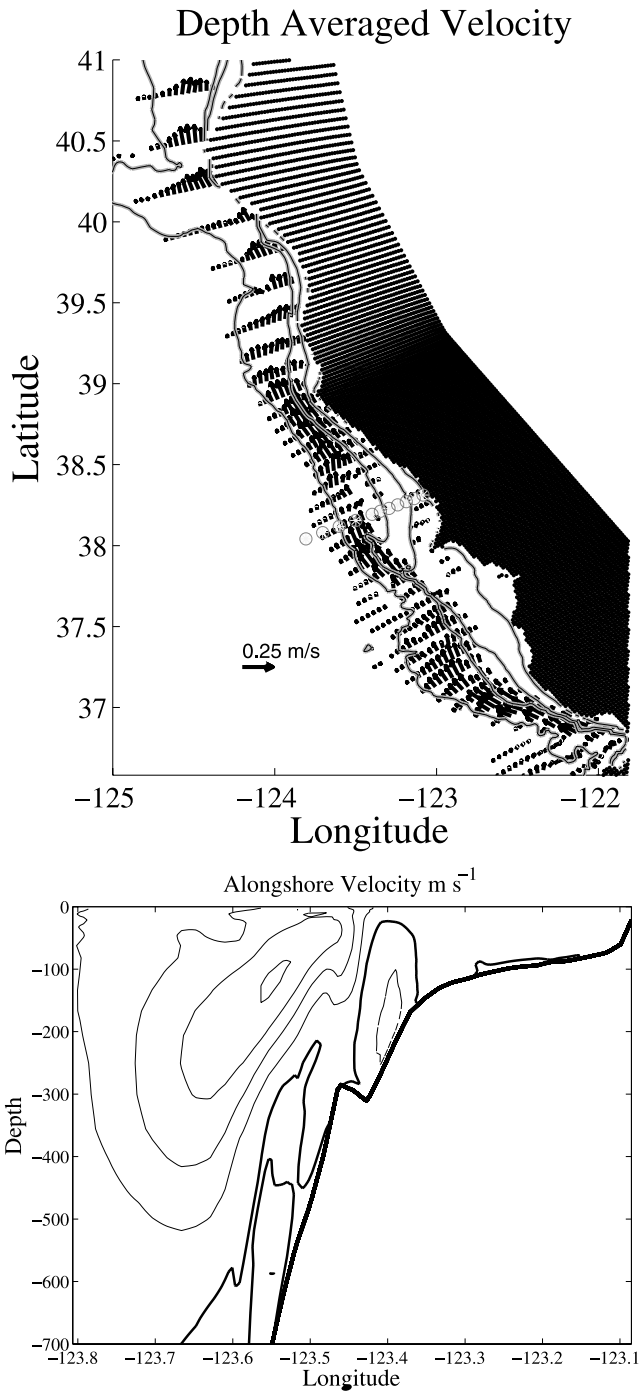

Figure 12. (top) The depth-averaged velocity of day 23 of the large model domain with a CUC forced by an inflow over the shelf of the southern boundary in a model run with no wind forcing. The 40, 90, 130, and 1200 m isobaths are shown. The stations of the "D-line" are indicated, and arrows are only drawn where the current is >2 cm s^{-1}. (bottom) The alongshore currents at the WEST D-line section defined by the central moorings and indicated Figure 12 (top). Positive isotachs are solid lines and represent poleward velocities. Negative isotachs are dashed, and the zero contour is a bold line. The contour interval for Figures 12 (top) and 12 (bottom) is 0.05 m s^{-1}.

did not affect along-coast pressure gradient in the vicinity of San Francisco, but did in other locations in Northern California and the Pacific Northwest. However, the alongshore pressure gradient does improve the agreement of the model to the observations near the shelf break by reducing the excessive poleward flow near the shelf break, as can be seen in Table 3 and Figure 4. *Noble and Ramp* [2000] observe that the flow associated with CUC can extend to the surface in this region (in the models this is true when the equatorward wind is weak).

[59] Both of these methods for setting up along-slope pressure gradients and CUC reduce the depth from which water is upwelled onto the shelf. The near bottom temperature at the central 90 m mooring is significantly warmer when there is a CUC and along-slope pressure gradient in the model (Figure 13), regardless of the method used to include them in the model. Also shown in Figure 13 are experiments run with stronger isopycnal tilts and weaker inflows in the southern boundary. In all cases the results are expected (a stronger along-slope pressure gradient and CUC allows warmer water to be upwelled onto the shelf).

[60] As discussed above, this effect can be quantified by examining the near bottom temperature. When the temperature reaches a steady state near the end of the model runs, it is consistent with upwelling from about 210 m depth in the model run forced with an isopycnal tilt, and 180 m in the model run forced with a southern inflow, as opposed to 300 m depth in the base model case and about 150 m in the observations. However, while estimates of upwelling based on near-bottom midshelf temperatures have the advantage of being directly comparable to observations, the effects of mixing in the bottom boundary layer and along-shelf advection can muddy their interpretation. By launching Lagrangian drifters in the numerical model, the source depth of the water can be directly estimated. The depths, not shown, are consistent with the depths given above, and confirm that greater alongshore poleward pressure gradients on the slope lead to water being upwelled from shallower depths. The observed change in temperature with changing along-slope pressure gradients is caused by a change in the depth from which water is upwelled from over the slope.

[61] These results only roughly indicate the impact of an alongshore pressure gradient on the source depth of upwelled waters. The source of the upwelled waters is controlled by the depth at which the vertical integral of the onshore geostrophic flow from the surface to that depth is equal to the offshore Ekman transport. This integral is sensitive to the vertical structure of the along-isobath pressure gradient over the slope. The vertical structure of the along-slope pressure gradient is set by the strength of the along-isobath sea surface height gradient and the vertical distribution of the along-isobath density gradient. These are very poorly constrained by the observations. Further, the observations of the CUC used to calibrate the alongshore pressure gradient in the model were taken in different years than those modeled. While it is possible to tune the model to match the WEST observations by altering the structure of the alongshore pressure gradient on the slope, the limited observations do not allow this to be done uniquely. There is simply too much uncertainty in the vertical and cross-slope structure of this alongshore pressure gradient for the WEST observations to constrain the pressure gradients. Any

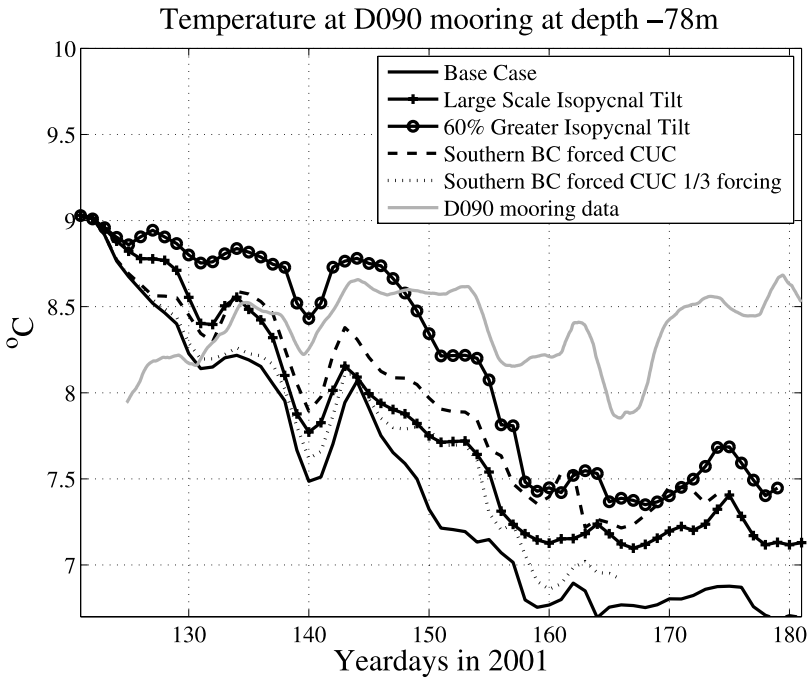

Figure 13. The 78 m depth temperature at the central mooring on the 90 m isobath as a function of time from the observations and from five model runs. The first run is the base large-domain case with spatially variable topography and COAMPS winds. The second includes uses the same domain and forcing, but includes a meridional gradient in waters deeper than 100 m as described in the text, in order to force a realistic CUC. The third run has a latitudinal gradient that is 60% greater than the second run. The fourth run includes a CUC forced with inflow over the shelf on the southern boundary, as detailed in the text. The fifth run is forced with a southern boundary shelf inflow 1/3 as great.

attempt to match the WEST observations would not be guaranteed to improve the model elsewhere or allow the model to correctly simulate quantities that we have not observed.

[62] Despite these caveats, historical works and these experiments suggest that the same processes that determine the along-slope pressure gradients and the strength of the CUC also control the source of the upwelled water. These processes are not captured by the short two-month integration of even the largest model domain. Only by including either larger-scale basin- or gyre-scale dynamics, or longer integrations, can we understand the processes that control the water masses upwelled onto the shelf, and perhaps their interannual variability. As the later is key to understanding many of the year to year ecological shifts on the shelf, it is likely that CUC/slope dynamics are a key link between long-timescale/large-scale dynamics and the shelf ecosystem.

8. Conclusions

[63] The upwelling response observed around Point Reyes during the WEST experiment is controlled by alongshore variation both in the bathymetry and in the alongshore wind field. These alongshore gradients cause weaker equatorward flows at the WEST site than would be expected from the local winds, and cause a gradient in the along-isobath flows, with weaker flows to the south and stronger flows to the north (Figure 7). The alongshore deceleration of the along-isobath flow appear in one-dimensional models such as *Lentz*'s [1994] as along-isobath pressure gradients that are strongly correlated to the alongshore wind, retard the flow, and vary on the same timescales as the wind.

[64] The spatial gradient in the alongshore flow is associated with stronger upwelling north of Point Reyes, and weaker upwelling to the south, leading to cooler and denser water to the north along the shelf. The poleward gradient in density also sets up an equatorward gradient in pressure that tends to drive poleward flows. This density gradient and the associated along-isobath pressure gradient persists on a timescale of 5 to 10 days, and drive the poleward flows on the shelf associated with upwelling relaxation. These relaxation flows exist in the model runs that do not contain an imposed large-scale along-slope pressure gradients, suggesting that basin-scale pressure gradients are not important to upwelling relaxation on the shelf during the late spring/early summer to midsummer upwelling season. This simple picture of the origin of alongshore pressure gradients and poleward relaxation flows is consistent with the earlier work of *Largier et al.* [1993] (their Figure 18) and *Hickey and Pola* [1983], who found that the poleward pressure gradients on shelf increase as the upwelling season progresses and the along-shelf density gradients and pressure gradients increase in strength. In the large domain model, there is a similar along-isobath density gradient caused by wind forcing on the shelf from Santa Barbara Channel to where the shelf becomes very narrow at about 35.75°N, suggesting that similar upwelling relaxation dynamics may be active in that region.

[65] The depth of the shelf waters upwelled onto the shelf, and thus the temperature and other properties of the

upwelled waters, are significantly modified by the large-scale poleward pressure gradient force over the slope adjacent to the Californian shelf. When the model is initialized with realistic meridional density gradients or with an inflow over the shelf on the southern model boundary, the model gains an along-slope pressure gradient and spins up a robust and realistic CUC. These changes lead to water being upwelled from a 100 m shallower depth in the model. The along-slope pressure gradient leads to a more realistic source depth for water upwelled onto the shelf because the along-slope pressure gradient drives an on-shelf geostrophic flow in the near surface waters on the slope which helps balance the offshore transport in the surface Ekman layer.

[66] The spatial scale of the dynamics discussed above can be used to determine the minimum size of model domain needed to accurately simulate both the shelf circulation and the upwelling of slope water onto the shelf. The circulation dynamics on the shelf are controlled by spatial gradients in the winds and bathymetry to the south. Model domains that do not include these gradients cannot reproduce all the features of the observed circulation, even if the local wind forcing and bathymetry are accurate. For example, the smallest of the model domains in Figure 1 does not include the extreme attenuation of the shelf and the region of weakest winds near Monterey Bay. Because of this, it fails to accurately reproduce the mean circulation strength near Point Reyes (Tables 1, 2, and 3). The medium sized domain, which extends to just south of Monterey Bay, does much better. It includes the region which *Denbo and Allen* [1987] find to dominate the wind forcing and also includes region of most dramatic variation in shelf width. The largest-scale model most accurately reproduces the alongshore currents in the Point Reyes region. This is consistent with findings of *Denbo and Allen* [1987] and others that there is poleward propagation of remotely forced CTW energy from the region around Point Conception north to Point Reyes. The along-slope pressure gradients offshore of the shelf break do not affect the circulation on the shelf in the WEST region, though, as can be seen in Figure 12, they can influence the shelf circulation elsewhere along the coast, in particular in the vicinity of Point Arena. However, in order to more accurately simulate the water masses upwelled onto the shelf from the slope, it is necessary to capture an even larger scale of variability (the scale of the dynamics that establish along-slope pressure gradients and a poleward undercurrent along the west coast of North America). Unfortunately, the dynamics leading to these phenomena are poorly understood, though there are some hints that basin-scale models can capture at least a part of them [*Garfield et al.*, 2001; *Choboter et al.*, 2002].

[67] Both the scale needed to capture the dynamics of the shelf currents and the scale needed to model the source of the upwelled water suggest that the 140 to 200 km along-shelf-scale circulation models that have been used to understand the phenomenology of shelf circulation on this coast are not adequate to quantitatively reproduce the details of shelf circulation here. Data assimilation that operates on the boundary conditions or boundary conditions taken from basin-scale models are necessary if one is to use regional-scale numerical models to accurately simulate shelf circulation.

[68] These results also emphasize the importance of highly resolved and accurate coastal wind fields to the successful modeling of coastal circulation in these complex domains (see *Cowles et al.* [2008] for a similar example from the Northeast Coast of North America). Numerical model runs forced with spatially uniform winds fail to reproduce the magnitude of the upwelling circulation. Even two high-resolution atmospheric models, the COAMPS model of NRL Monterey [*Haack et al.*, 2005] and the MM5 model of *Koracin et al.* [2004], both well validated against observations, can produce significantly different flow fields when applied to the ocean circulation model. In this application, the MM5 model has weaker winds over the ocean, but weaker cross-shelf gradients in the along-shelf winds. This leads to reduced and less realistic cross-shelf gradients in the along-shelf currents (Tables 1, 2, and 3), and improved temperatures on the shelf (the water is upwelled from about 40 m less deep on the slope). Determining the ''best'' atmospheric model for the forcing of ocean model is difficult, given the limited observational base that can be used to compare each model to observation, and given the difficulties in comparing observations of wind speed to estimates of wind stress.

[69] Nonetheless, these results suggest that there is a need for the development and routine use of large-scale coastal ocean models into which more highly resolved coastal models can be nested, and the development and routine use of highly resolved coastal atmospheric models with which to force these models. While limited domain shelf scale models forced by point observations of the winds have proved valuable in understanding the basic dynamics of wind-driven coastal flows, they will miss important regional scale dynamics that lead to qualitatively important phenomena such as upwelling relaxation. Likewise, small-scale models that can satisfactorily resolve the flow on the shelf in this region will fail to resolve the connection of these flows to the deeper ocean, and will not reproduce the important fluxes of heat, carbon, nutrients and biota between the deep ocean and the shelf.

[70] **Acknowledgments.** This work was only possible because of many different data and modeling efforts that have come before it. The COAMPS winds were courtesy of the Navy Research Laboratory in Monterey and were made available to me by Tracy Haack. The MM5 winds were made available to me by Darko Koracin and Clive Dorman. All of them made time to explain to me the details of the their models and their relative strengths and weaknesses. Of course, none of this paper would have been possible without the tremendous work of the all the participants in the WEST projects. In particular, David Kaplan shared his CODAR data, and Moninya Roughan was generous in explaining her work to us. The modeling built on previous efforts, and Brandy Kuebel-Cervantes was generous in describing what she had done and the pitfalls in modeling this area. This work was funded by NSF as parts of OCE-0453792 and OCE-9907884. Ken Brink made numerous helpful suggestions on an early version of the paper, and Steve Lentz helped the paper with several perceptive and useful comments.

References

Allen, S. (2000), On subinertial flow in submarine canyons: Effect of geometry, *J. Geophys. Res.*, *105*, 1285–1297.

Antonov, J. I., R. A. Locarnini, T. P. Boyer, A. V. Mishonov, and H. E. Garcia (2006), *World Ocean Atlas 2005*, vol. 2, *Salinity*, *NOAA Atlas NESDIS*, vol. 62, edited by S. Levitus, 182 pp., NOAA, Silver Spring, Md.

Austin, J., and S. Lentz (2002), The inner shelf response to wind-driven upwelling and downwelling, *J. Phys. Oceanogr.*, *32*, 2171–2193.

Bray, N. A., and C. L. Greengrove (1993), Circulation over the shelf and slope off Northern California, *J. Geophys. Res.*, *98*, 18,119–18,145.

Brown, W. S., J. D. Irish, and C. D. Winant (1987), A description of subtidal pressure field observations on the northern California continental-shelf during the Coastal Ocean Dynamics Experiment, *J. Geophys. Res.*, *92*, 1605–1635.

Cervantes, B. T. K., and J. S. Allen (2006), Numerical model simulations of continental shelf flows off northern California, *Deep Sea Res., Part II*, *53*, 2956–2984.

Chapman, D. (1986), A simple model of the formation and maintenance of the shelf/slope front in the Middle Atlantic Bight, *J. Phys. Oceanogr.*, *16*, 1273–1279.

Chapman, D. (1987), Application of wind-forced, long, coastal-trapped wave theory along the California coast, *J. Geophys. Res.*, *92*, 1798–1816.

Chapman, D. C. (2003), Separation of an advectively trapped buoyancy current at a bathymetric bend, *J. Phys. Oceanogr.*, *33*, 1108–1121.

Chapman, D. C., S. J. Lentz, and K. H. Brink (1988), A comparison of empirical and dynamical hindcasts of low-frequency, wind-driven motions over a continental shelf, *J. Geophys. Res.*, *93*, 12,409–12,422.

Choboter, P., J. Allen, and R. Samelson (2002), Model dynamical balances within the California undercurrent, *Eos Trans. AGU*, *83*(47), Fall Meet. Suppl., Abstract OS62A-0243.

Clarke, A. J., and M. Dottori (2008), Planetary wave propagation off California and its effect on zooplankton, *J. Phys. Oceanogr.*, *38*, 702–714.

Clarke, A. J., and S. VanGorder (1986), A method for estimating wind-driven frictional, time-dependent, stratified shelf and slope water flow, *J. Phys. Oceanogr.*, *16*, 1013–1028.

Cowles, G. W., S. J. Lentz, C. Chen, Q. Xu, and R. Beardsley (2008), Comparison of observed and model-computed low frequency circulation and hydrography on the New England Shelf, *J. Geophys. Res.*, *113*, C09015, doi:10.1029/2007JC004394.

Csanady, G. (1978), The arrested topographic wave, *J. Phys. Oceanogr.*, *8*, 47–62.

Denbo, D., and J. Allen (1987), Large-scale response to atmospheric forcing of shelf currents and coastal sea level off the west coast of North America: May–July 1981 and 1982, *J. Geophys. Res.*, *92*, 1757–1782.

Dever, E. (1997), Wind-forced cross-shelf circulation on the Northern California Shelf, *J. Phys. Oceanogr.*, *27*, 1566–1579.

Dever, E., and S. Lentz (1994), Heat and salt balances over the Northern California Shelf in winter and spring, *J. Geophys. Res.*, *99*, 16,001–16,017.

Dever, E. P., C. E. Dorman, and J. L. Largier (2006), Surface boundary-layer variability off Northern California, USA, during upwelling, *Deep Sea Res., Part II*, *53*, 2887–2905.

Dong, C., and L. Oey (2005), Sensitivity of coastal currents near Pt. Conception to forcing by three different winds: ECMWF, COAMPS and blended SSM/I-ECMWF-buoy winds, *J. Phys. Oceanogr.*, *35*, 1229–1244.

Enfield, D., and J. Allen (1980), On the structure and dynamics of monthly mean sea level anomalies along the Pacific coast of North and South America, *J. Phys. Oceanogr.*, *10*, 557–578.

Gan, J., and J. Allen (2002a), A modeling study of shelf circulation off northern California in the region of the Coastal Ocean Dynamics Experiment 2. Simulation and comparisons with observations, *J. Geophys. Res.*, *107*(C11), 3184, doi:10.1029/2001JC001190.

Gan, J. P., and J. S. Allen (2002b), A modeling study of shelf circulation off northern California in the region of the Coastal Ocean Dynamics Experiment: Response to relaxation of upwelling winds, *J. Geophys. Res.*, *107*(C11), 3184, doi:10.1029/2001JC001190.

Gan, J., and J. S. Allen (2005), On open boundary conditions for a limited-area coastal model off Oregon. Part 1: Response to idealized wind forcing, *Ocean Modell.*, *8*, 115–133.

Garcia, H. E., R. A. Locarnini, T. P. Boyer, and J. I. Antonov (2006a), *World Ocean Atlas 2005*, vol. 3, *Dissolved Oxygen, Apparent Oxygen Utilization, and Oxygen Saturation*, *NOAA Atlas NESDIS*, vol. 63, edited by S. Levitus, 342 pp., NOAA, Silver Spring, Md.

Garcia, H. E., R. A. Locarnini, T. P. Boyer, and J. I. Antonov (2006b), *World Ocean Atlas 2005*, vol. 4, *Nutrients (Phosphate, Nitrate, and Silicate)*, *NOAA Atlas NESDIS*, vol. 64, edited by S. Levitus, 396 pp., NOAA, Silver Spring, Md.

Garfield, N., M. E. Maltrud, C. A. Collins, T. A. Rago, and R. G. Paquette (2001), Lagrangian flow in the California Undercurrent, an observation and model comparison, *J. Mar. Syst.*, *29*, 201–220.

Haack, T., S. D. Burk, and R. M. Hodur (2005), U.S. West Coast surface heat fluxes, wind stress, and wind stress curl from a mesoscale model, *Mon. Weather Rev.*, *133*, 3202–3216.

Hickey, B., and N. Pola (1983), The seasonal alongshore pressure gradient on the West Coast of the United States, *J. Geophys. Res.*, *88*, 7623–7633.

Hill, A. E. (1995), Leakage of barotropic slope currents onto the continental shelf, *J. Phys. Oceanogr.*, *25*, 1617–1621.

Huthnance, J. M. (1984), Slope currents and "JEBAR", *J. Phys. Oceanogr.*, *14*, 795–810.

Janowitz, G., and L. Pietrafesa (1982), The effects of alongshore variation in bottom topography on a boundary current — (Topographically induced upwelling), *Cont. Shelf Res.*, *1*, 123–141.

Kantha, L. H., and C. A. Clayson (1994), An improved mixed-layer model for geophysical applications, *J. Geophys. Res.*, *99*, 25,235–25,266.

Kaplan, D. M., J. Largier, and L. W. Botsford (2005), HF radar observations of surface circulation off Bodega Bay (northern California, USA), *J. Geophys. Res.*, *110*, C10020, doi:10.1029/2005JC002959.

Koracin, D., C. E. Dorman, and E. P. Dever (2004), Coastal perturbations of marine-layer winds, wind stress, and wind stress curl along California and Baja California in June 1999, *J. Phys. Oceanogr.*, *34*, 1152–1173.

Kuebel-Cervantes, B., and E. Dever (2006), Numerical modeling of the circulation over the continental shelf off northern California, *Eos Trans. AGU*, *87*(36), Ocean Sci. Meet. Suppl., Abstract OS36D-15.

Large, W., and S. Pond (1981), Open ocean momentum flux measurements in moderate to strong winds, *J. Phys. Oceanogr.*, *11*, 324–336.

Largier, J. L., B. A. Magnell, and C. D. Winant (1993), Subtidal circulation over the Northern California shelf, *J. Geophys. Res.*, *98*, 18,147–18,179.

Largier, J. L., et al. (2006), WEST: A northern California study of the role of wind-driven transport in the productivity of coastal plankton communities, *Deep Sea Res., Part II*, *53*, 2833–2849.

Lentz, S. (1987), A description of the 1981 and 1982 spring transitions over the northern California shelf, *J. Geophys. Res.*, *92*, 1545–1567.

Lentz, S. J. (1994), Current dynamics over the northern California inner-shelf, *J. Phys. Oceanogr.*, *24*, 2461–2478.

Lentz, S. (2008), Observations and a model of the mean circulation over the Middle Atlantic Bight Continental Shelf, *J. Phys. Oceanogr.*, *38*, 1203–1221.

Lentz, S., and D. Chapman (2004), The importance of non-linear cross-shelf momentum flux during wind-driven coastal upwelling, *J. Phys. Oceanogr.*, *34*, 2444–2457.

Lentz, S., and J. Trowbridge (2001), A dynamical description of fall and winter mean current profiles over the northern California Shelf, *J. Phys. Oceanogr.*, *31*, 914–931.

Locarnini, R. A., A. V. Mishonov, J. I. Antonov, T. P. Boyer, and H. E. Garcia (2006), *World Ocean Atlas 2005*, vol. 1, *Temperature, NOAA Atlas NESDIS*, vol. 61, edited by S. Levitus, 182 pp., NOAA, Silver Spring, Md.

Lopez-Mariscal, M., and A. Clarke (1993), On the influence of wind-stress curl on low-frequency shelf water-flow, *J. Phys. Oceanogr.*, *23*, 2717–2727.

Louis, J. F. (1979), Parametric model of vertical eddy fluxes in the atmosphere, *Boundary Layer Meteorol.*, *17*, 187–202.

Marchesiello, P., J. C. Mcwilliams, and A. Shchepetkin (2003), Equilibrium structure and dynamics of the California Current system, *J. Phys. Oceanogr.*, *33*, 753–783.

McCreary, J. P. (1981), A linear stratified ocean model of the coastal undercurrent, *Philos. Trans. R. Soc. London, Ser. A*, *302*, 385–413.

McCreary, J., and S.-Y. Chao (1985), Three-dimensional shelf circulation along an eastern ocean boundary, *J. Mar. Res.*, *43*, 13–36.

McCreary, J., P. Kundu, and S. Chao (1987), On the dynamics of the California Current System, *J. Mar. Res.*, *45*, 1–32.

McCreary, J. P., Y. Fukamachi, and P. Lu (1991), A nonlinear mechanism for maintaining coastally trapped Eastern Boundary Currents, *J. Geophys. Res.*, *97*, 5677–5692.

Mellor, G., and T. Yamada (1982), Development of a turbulance closure model for geophysical fluid problems, *Rev. Geophys.*, *20*, 851–875.

Mellor, G. L., T. Ezer, and L. Y. Oey (1994), The pressure-gradient conundrum of sigma coordinate ocean models, *J. Atmos. Oceanic Technol.*, *11*, 1126–1134.

Middleton, J. H. (1987), Steady coastal circulation due to oceanic alongshore pressure gradients, *J. Phys. Oceanogr.*, *17*, 604–612.

Neshyba, S. J., C. N. K. Mooers, R. L. Smith, and R. T. Barber (Eds.) (1989), *Poleward Flows Along Eastern Ocean Boundaries*, *Coastal Estuarine Stud.*, vol. 34, AGU, Washington, D. C.

Noble, M. A., and S. R. Ramp (2000), Subtidal currents over the central California slope: Evidence for offshore veering of the undercurrent and for direct, wind-driven slope currents, *Deep Sea Res., Part II*, *47*, 871–906.

Oey, L.-Y. (1999), A forcing mechanism for the poleward flow off the southern California coast, *J. Geophys. Res.*, *104*, 13,529–13,539.

Oey, L.-Y., C. Winant, E. Dever, W. Johnson, and D. Wang (2004), A model of the near-surface circulation of the Santa Barbara Channel: Comparison with observations and dynamical interpretations, *J. Phys. Oceanogr.*, *34*, 23–43.

Pierce, S. D., R. L. Smith, P. M. Kosro, J. A. Barth, and C. D. Wilson (2000), Continuity of the poleward undercurrent along the eastern boundary of the mid-latitude north Pacific, *Deep Sea Res., Part II*, *47*, 811–829.

Pringle, J. (2002), Enhancement of wind-driven upwelling and downwelling by alongshore bathymetric variability, *J. Phys. Oceanogr.*, *32*, 3101–3112.

Reid, J. L., and A. W. Mantyla (1976), Effect of geostrophic flow upon coastal sea elevations in northern North Pacific Ocean, *J. Geophys. Res.*, *81*, 3100–3110.

Roughan, M., N. Garfield, J. Largier, E. Dever, C. Dorman, D. Peterson, and J. Dorman (2006), Transport and retention in an upwelling region: The role of across-shelf structure, *Deep Sea Res., Part II*, *53*, 2931–2955.

Send, U., R. C. Beardsley, and C. D. Winant (1987), Relaxation from upwelling in the coastal ocean dynamics experiment, *J. Geophys. Res.*, *92*, 1683–1698.

Shaw, P. T., and G. T. Csanady (1983), Self-advection of density perturbations on a sloping continental shelf, *J. Phys. Oceanogr.*, *13*, 769–782.

Shchepetkin, A. F., and J. C. McWilliams (2003), A method for computing horizontal pressure-gradient force in an oceanic model with a nonaligned vertical coordinate, *J. Geophys. Res.*, *108*(C3), 3090, doi:10.1029/2001JC001047.

Strub, P., J. Allen, A. Huyer, R. Smith, and R. Beardsley (1987), Seasonal cycles of currents, temperatures, winds, and sea level over the northeast Pacific continental shelf: 35°N to 48°N, *J. Geophys. Res.*, *92*, 1507–1526.

Vennell, R., and P. Malanotte-Rizzoli (1987), Coastal flows driven by alongshore density gradients, *J. Phys. Oceanogr.*, *17*, 821–827.

Werner, F. E., and B. M. Hickey (1983), The role of a longshore pressure-gradient in Pacific Northwest coastal dynamics, *J. Phys. Oceanogr.*, *13*, 395–410.

Wilkin, J., and D. Chapman (1990), Scattering of coastal-trapped waves by irregularities in coastline and topography, *J. Phys. Oceanogr.*, *20*, 396–421.

Winant, C. (1979), Comments on ''The arrested topographic wave,'' *J. Phys. Oceanogr.*, *9*, 1042–1043.

Winant, C., R. Beardsley, and R. Davis (1987), Moored wind, temperature, and current observations made during coastal ocean dynamics experiments 1 and 2 over the northern California continental shelf and upper slope, *J. Geophys. Res.*, *92*, 1569–1604.

Wing, S. W., L. W. Botsford, J. L. Largier, and L. E. Morgan (1995), Spatial structure of relaxation events and crab settlement in the northern California upwelling system, *Mar. Ecol. Prog. Ser.*, *128*, 199–211.

Wright, D. G. (1986), On quasi-steady shelf circulation driven by alongshelf wind stress and open-ocean pressure gradients, *J. Phys. Oceanogr.*, *16*, 1712–1714.

Zamudio, L., and M. Lopez (1994), On the effect of the alongshore pressure gradient on numerical simulations over the northern California continental shelf, *J. Geophys. Res.*, *99*, 16,117–16,129.

E. P. Dever, College of Oceanic and Atmospheric Sciences, Oregon State University, 104 COAS Administration Building, Corvallis, OR 97331-5503, USA. (edever@coas.oregonstate.edu)

J. M. Pringle, Department of Earth Sciences, UNH, 142 Morse Hall, 39 College Street, Durham, NH 03824-3525, USA. (jpringle@unh.edu)